Comparative study of low cost, eco-friendly and high performance biowastes-derived porous activated carbons for symmetric supercapacitors

By

Rabia Fatima

Regn no: 00000327074

Master of Science in Industrial Biotechnology

Supervisor:

Dr. Saadia Andleeb

Department of Industrial Biotechnology

Atta-ur-Rahman School of Applied Biosciences (ASAB)

National University of Sciences and Technology (NUST)

Islamabad, Pakistan

September, 2022.

Comparative study of low cost, eco-friendly and high performance biowastes-derived porous activated carbons for symmetric supercapacitors

By

Rabia Fatima

Regn no: 00000327074

Master of Science in Industrial Biotechnology

Supervisor:

Dr. Saadia Andleeb

Co-Supervisor:

Dr. Farooq Sher

Department of Industrial Biotechnology

Atta-ur-Rahman School of Applied Biosciences (ASAB)

National University of Sciences and Technology (NUST)

Islamabad, Pakistan

September, 2022.

Comparative study of low cost, eco-friendly and high performance biowastes-derived porous activated carbons for symmetric supercapacitors

A thesis submitted in partial fulfilment of the requirement for the degree

of Master of Science (MS)

In

Industrial Biotechnology

By

Rabia Fatima

Registration No. 00000327074

Supervised by

Dr. Saadia Andleeb

Supervisor's Signature _____

Department of Industrial Biotechnology

Atta-ur-Rahman School of Applied Biosciences (ASAB)

National University of Sciences and Technology (NUST)

Islamabad, Pakistan

September, 2022.

Thesis Acceptance Certificate

It is certified that the contents of thesis entitled **"**Comparative study of low cost, eco-friendly and high performance biowastes-derived porous activated carbons for symmetric supercapacitors**"** submitted by **Rabia Fatima, Registration no. 00000327074** of **ASAB** has been found satisfactory for the requirement of the degree.

_____

Supervisor: Dr. Saadia Andleeb

Atta-ur-Rahman School of Applied Biosciences

National University of Science and Technology

_____

Head of Department: Dr. Amjad Ali

Atta-ur-Rahman School of Applied Biosciences

National University of Science and Technology

_____

Principal: Dr. Hussnain Janjua

Atta-ur-Rahman School of Applied Biosciences

National University of Science and Technology

Certificate of Plagiarism

It is to confirm that MS thesis entitled "Comparative study of low cost, eco-friendly and high performance biowastes-derived porous activated carbons for symmetric supercapacitors" of **Ms. Rabia Fatima**, **Registration no. 00000327074** of **ASAB** has been examined by me. I undertake that,

1. Thesis has significant new work/knowledge as compares to already elsewhere. No sentence, table, equation, diagram, paragraph, or section has copied verbatim from previous work except when placed under quotation marks and duly referenced.

2. The work presented is original and own work of author i.e., there is no plagiarism. No idea, results or work of others have been presented as author's own work.

3. There is no fabrication of data or results such that the research is not accurately represented in the records. The thesis has been checked using Turnitin, a copy of the originally report attached and focused within the limits as per HEC plagiarism policy and instruction based on time to time.

_____

(Supervisor)
Dr. Saadia Andleeb
Professor, ASAB, NUST.

Copyright statement

- Copyright in text of this thesis rests with the student Rabia Fatima. Copies (by any process) either in full, or of extracts may be made only in accordance with instruction given by the author and lodged in the library of Atta-ur-Rahman School of Applied Biosciences (ASAB). Details may be obtained by the librarian. This page must find part of any such copies made further copies (by any process) may not be made without the permission (in writing) of the author.
- The ownership of any intellectual property rights which may be described in this thesis is vested in Atta-ur-Rahman School of Applied Biosciences (ASAB) National University of Science and Technology (NUST), subject to any prior agreement to the contrary, and may not be made available for use by third parties without the written permission of the ASAB, which will describe the terms and condition of any such agreement.
- Further information on the conditions under which disclosures and exploitation may take place is available from the library of Atta-ur-Rahman School of Applied Biosciences (ASAB), Islamabad.

Declaration

I, **Rabia Fatima,** declare that this research work titled "Comparative study of low cost, eco-friendly and high performance biowastes-derived porous activated carbons for symmetric supercapacitors" is my own work. The work has not been presented elsewhere for assessment. The work here in was carried out while I was a post-graduate student at Atta-ur-Rahman School of Applied Biosciences, NUST under the supervision of Dr. Saadia Andleeb. The material that has been used from other sources has been properly acknowledged / referred.

Rabia Fatima

00000327074

Dedication

I, with great pleasure and reverence, dedicate this work to the Holy Prophet (P.B.U.H) who inspired me through His saying "*Learn from cradle to grave*".

Acknowledgements

I would like to convey my deepest appreciation to Prof. Saadia Andleeb, Dr. Farooq Sher and Dr. Muhammad Bilal Khan Niazi for providing their constant encouragement, invaluable guidance, monthly feedbacks, helpful discussions, patience and understanding throughout my MS research project and for taking over as my supervisors towards the final stages of my MS despite their busy schedule. Without their help, this research work would not have been completed.

A further appreciation goes to my senior Sir Armaan for his technical support and advice during my electrochemical testings. Special thanks to Muhammad Ali for his endless support and guidance with the OriginPro software. Also, I would like to acknowledge all the lab engineers in the School of Chemical and Material Engineering department (SCME) who performed all the characterizations of my samples i. e. Raman Spectroscopy, SEM-EDX, XRD, and FTIR etc. Appreciations also go to USP-CASE for providing the TGA & BET facility at National University of Science and Technology (NUST), Pakistan.

To my dearest friends, Safa Mariyam, Syeda Duaa, Mahnoor Khan and Ayesha Gul who are also pursuing their MS at the Atta-ur-Rehman School of Applied Biosciences (ASAB), much thanks for your unmatchable positive support, helpful suggestions, extensive concern and kind understanding despite the stress/challenges that you are coping in your research. I feel myself very lucky to have you amazing peeps by my side and I cherish every single moment of your time.We had the privilege of growing up every day both professionally as well as personally that I would definitely miss out. I would like to express my deepest appreciation to my friend, Umar Shah, who have supported and nurtured throughout the peak levels of depression during this endeavor. Thank you for your unwavering support, helpful advices and for reminding me to take breaks and have fun when I've been entirely stressed out.

Finally, I would like to thank my family who have been my pillars of strength, have encouraged and supported my research undertakings. It is no exaggeration to say that I could not have been able to complete the MS work without their generous help and constant encouragements.

Thank you also to those I have failed to mention, but who have contributed directly or indirectly toward the production of my thesis.

Table of Contents

List of Figures

List of Tables

List of Acronyms

SSA	Specific Surface area
NPC	Nano-porous carbons
AC-C	Activated carbon maize cob
SC-C	Simple carbon maize cob
AC-W	Activated carbon wood scraps
SC-W	Simple carbon wood scraps
KOH	Potassium hydroxide
HCl	Hydrochloric acid
XRD	X-Ray Diffraction
SEM	Scanning Electron Microscopy
EDX	Elemental dispersive X-ray
TGA	Thermogravimetric analysis
FTIR	Fourier transform infrared
CV	Cyclic voltammetry
GCD	Galvanostatic charge discharge
EIS	Electrochemical impedance spectroscopy

Abstract

Porous materials particularly, nano-porous carbons are well known because of having high specific surface area (SSA), different pore dimensions, inherent excellent conductance, low density, and highly available. The most effective source of cheap, plentiful, and environmentally safe precursors for nano-porous carbon, which are then used in energy storage technologies like high-performance symmetric supercapacitors, has been found to be 'biowaste/biomass'. This study compares two different biowastes-derived porous carbons such as wood and maize cobs using a straightforward one-step pyrolysis and potassium hydroxide (KOH) activation method for use in symmetric supercapacitors. Using XRD, SEM-EDX, FTIR, TGA, and subsequent CV, GCD, EIS, and cycle stability testing, the microstructures, morphology, and comparative study on electrochemical performance of resulting activated carbons were analyzed. The prepared carbon electrode made from maize cobs and wood scraps exhibits an electrical conductivity of 535.75 $F.g^{-1}$ and 135.64 $F.g^{-1}$ at 5 $A.g^{-1}$ in a 6 M KOH electrolyte as a result. The samples also showed a remarkable cycling stability of 99.81 % and 97.67 % at 10 k cycles. In conclusion, the higher electrochemical behavior of carbon material made from maize cobs in comparison to wood scraps can be due to the combination of a high specific surface area with a large number of mesopores/micropores and a highly stable structure.

***Keywords*:** nano-porous carbon, SSA, electrical conductivity, eco-friendly, low cost, highly conductive, symmetric supercapacitor, corncob/wood, KOH activation

CHAPTER 1

Introduction

1.1 General Background

The nano-porous materials are capable of interaction with molecules due to having vast inner surface and constrained nano-structures makes them of significant scientific and technological significance. They demonstrate their potential impact on a broad range of research fields, including electrical devices to meet the ever-growing need of energy, their special attributes, which open up new opportunities in the field of chemistry. The fascinating chemical and physical properties of nano-porous carbons (NPCs), which have interpenetrating and regular nanopore systems, including higher specific surface area (SSA), pore structure, higher heat and chemical stability, higher electrical conductivity, and abundancy, have recently sparked enormous research activity. As a result, they have been used in electrochemical, energy conversion, and storage technologies.

Recently, a lot of research has been put into developing new, low-cost, eco-friendly synthetic approaches that can be bioprocessed for mass production, as well as improving existing fabrication techniques for carbon. Researcher's interest has recently been drawn to porous carbons made from biowaste for a variety of applications. Biowaste is a more promising precursor than its rivals because it is easily accessible and produces porous carbon that is not only economical but also environmentally friendly.

In my master's thesis, I developed a synthesis method to create highly functional porous carbons with a large surface area from the readily available and affordable biowaste precursors "maize cob & wood waste." My main goal is to concentrate on a synthesis route that is straightforward, affordable, and easily scale-able for commercial production. Another focus of my research is the optimization of the synthesis conditions. By carefully adjusting the synthesis conditions, I produced porous carbons having a high SSA. While simultaneously lowering the overall production expenditure and environmentally viable. Utilizing X-ray diffraction (XRD), scanning electron microscopy (SEM), elemental dispersive X- ray (EDX), Fourier transform infrared spectroscopy (FTIR), thermogravimetric analysis (TGA), Raman spectroscopy, and other techniques, structural and morphological analysis of the synthesized biowastes-derived porous carbons was done. The ultimate objective was to incorporate the nano-porous carbons derived from biowaste into real- world applications, such as energy applications i. e. supercapacitors, and to track the structural variables that influence its general performance in

the targeted application.

1.2 Nano-porous materials

Due to their numerous practical uses in energy storage devices such as lithium ion batteries, lithium sulphur batteries, sodium ion batteries etc. Moreover, nowadays are being used in supercapacitors, energy conversion in fuel cells, hydrogen storage, solar cells, and other processes, nano-porous materials termed as more advantageous to 21st century technology [1]. Because of having special characteristics, nano-porous materials enable a diverse range of applications. In general, macro-porous (>50 nm), mesoporous (2 nm to 50 nm), and microporous (2 nm) types of nano-porous materials can be distinguished [2].

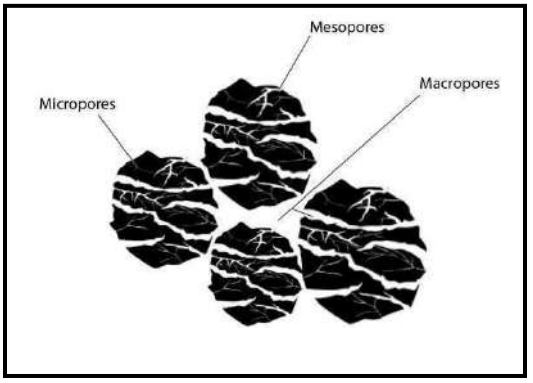

Figure 1. Illustration of the various pore configurations of a general carbon material.

The illustration of the different pore arrangements in a common carbon material is shown in figure 1. Nano-porous carbons (NPCs), which are among the many porous materials, have drawn attention from researchers because of their intriguing chemical and physical characteristics, including their high surface area, high thermal and chemical stability, changeable pore structure, excellent electrical conductivity, and widespread availability [3]. As a result, it has been crucial to optimize the current synthesis process and introduce new synthesis methods for nano-porous carbon. Conventional porous carbon materials, such as activated carbon, are frequently made by subjecting organic precursors, such as coal, wood, or polymers, to pyrolysis or hydrothermal treatment followed by chemical or physical activation at high temperatures [4]. Large-scale production of porous carbon materials with large surface areas has led to their widespread use in energy storage and conversion technologies [5].

Biomass has recently been used as an economical and environmentally friendly precursor for the creation of nano-porous carbon [6]. The term "biomass" refers to materials that can be used to synthesize carbon materials for a variety of applications that are derived from either plants or

animals, plants, animals, industrial processes, or sewage or municipal waste. These types of biomasses are also referred to as lignocellulose and are composed of aromatic and carbohydrate polymers (cellulose and hemicellulose). Because the biomass precursors are rich in carbon, they can be synthesized to create carbon materials with unique properties.

The formation of high surface area and porosity in the carbon material is one significant characteristic that is of high interest [7]. Direct pyrolysis or hydrothermal carbonization, followed by activation of the carbon to significantly increase the surface area, are the two main techniques for producing porous carbon materials.

1.3 Global Energy Demand

On the other hand, energy is the main force behind global economic and social growth that is sustainable. Fossil fuels are the main primary sources for the industrial, transportation, electricity, commercial, and residential sectors in the world, according to BP 2017 data [8], which accounts for87% of global energy consumption in 2015. The World Energy Council (2013) [9] predicted that, as a result of the growing global population, energy consumption will nearly double by 2050 compared to today's levels. Global energy demand is being met by cleaner energy sources thanks toa sharp rise in energy consumption worldwide and thedepletion of fossil fuels. According to the most recent BP Energy Outlook 2017, the world's energy demand is expected to rise by 30% by the year 2035, and renewable energy is predictedto grow at the fastest rate (7.6% on average annually), coming from sources like solar, geothermal, biomass, biofuels, and wind energy (Figure 2).

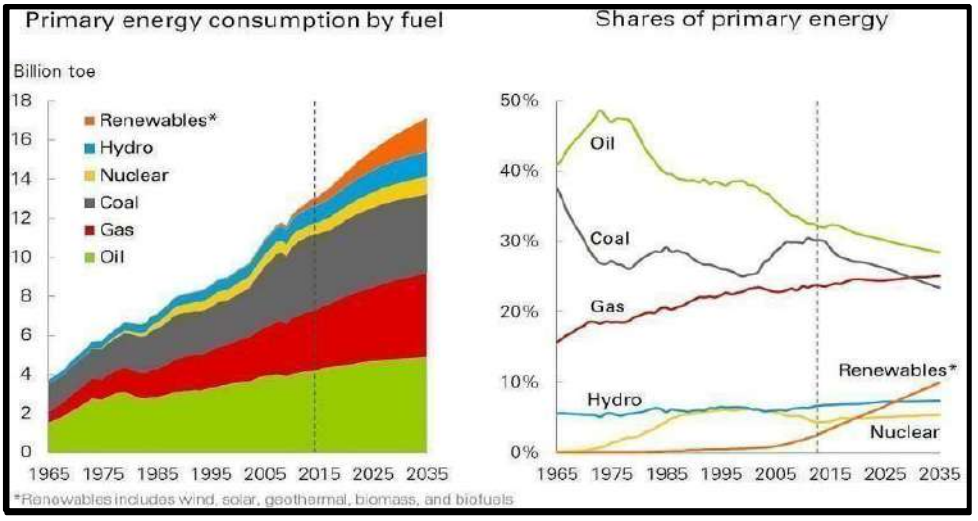

Figure 2. Global energy consumption and shares of primary energy in 1965 to 2015 and projections until 2035. [8]

According to Figure 3, the primary production of energy from renewable sources increased by three times in the European Union (EU) countries in 2016 compared to its value in 1990. In comparison to 1995, the EU projects that its renewable energy production from wind, biomass, and hydro will increase by almost four times by 2020. In this situation, energy storage devices like supercapacitors can help maintain a stable and safe electricity supply by balancing the power grids. During the energy harvesting period, electricity from intermittent power sources, such as wind, tidal, and solar power, can be stored in an energy storage system to maintain the supply of energy to demand when the production falls below the consumption.

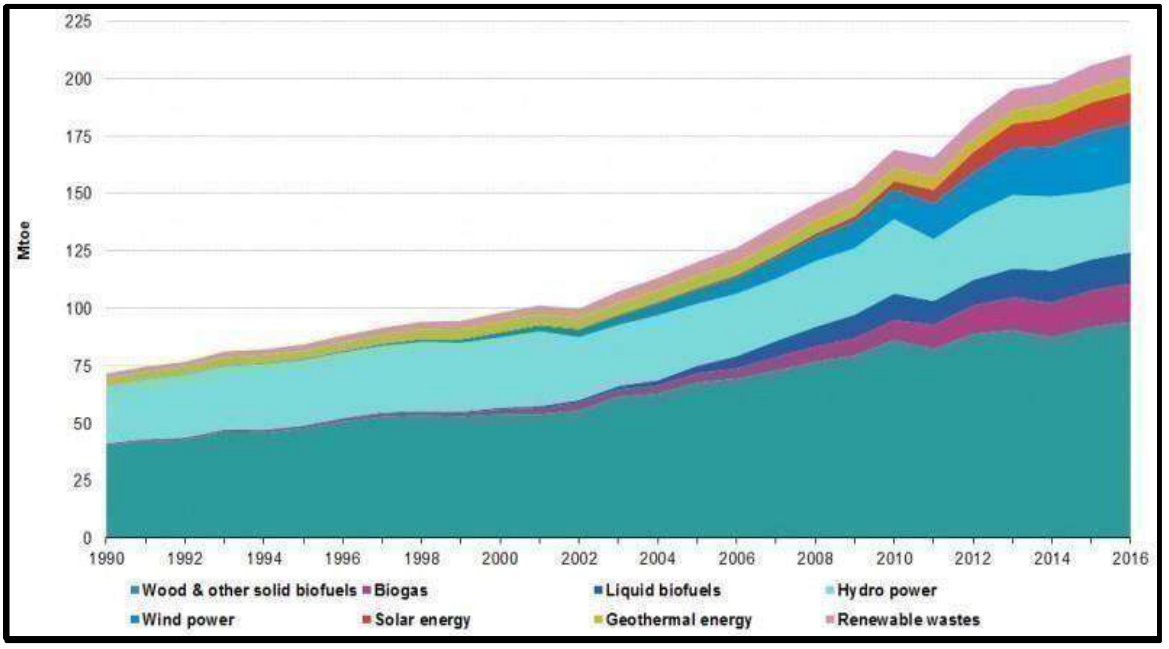

Figure 3. Primary production of energy from renewable sources EU 1990-2016 [10]

Additionally, it is more practical to integrate smaller, lighter, and thinner energy storage systems with today's electronic gadgets, such as laptops, smartphones, notepads, global positioning systems, etc. In spite of power outages, users are still able to carry and use their portable electronics.

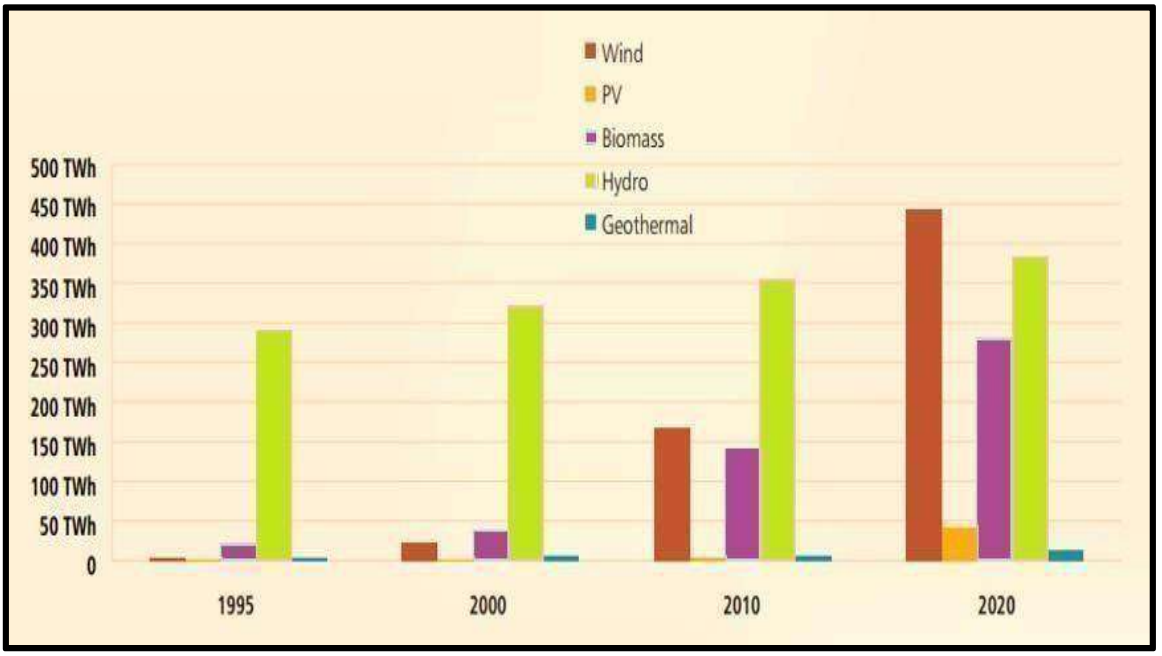

Figure 4. EU target for renewable energy production (1995 to 2020) [11]

1.4 Supercapacitor (Energy storage system)

The supercapacitor (also referred to as an electric double layer capacitor, or EDLC), which has the potential in the aforementioned applications, is an energy storage system with a higher cycling efficiency (98%), an improved power density, and a better cycle lifetime (10^6) than batteries.

In 2024, the supercapacitor market is projected to reach a value of $6 billion USD, with a 30% compound annual growth rate over the following ten years, according to one of the European market research firms, IDTechEx [13]. The market is anticipated to continue to grow in the transportation and grid levelling sectors (Figure 5). The hybrid Toyota TS040 racing car can be used as a temporary four-wheel drive by using an additional supercapacitor system to increase the engine power from 530 HP to 830 HP. This application has been demonstrated in real-world vehicle applications.

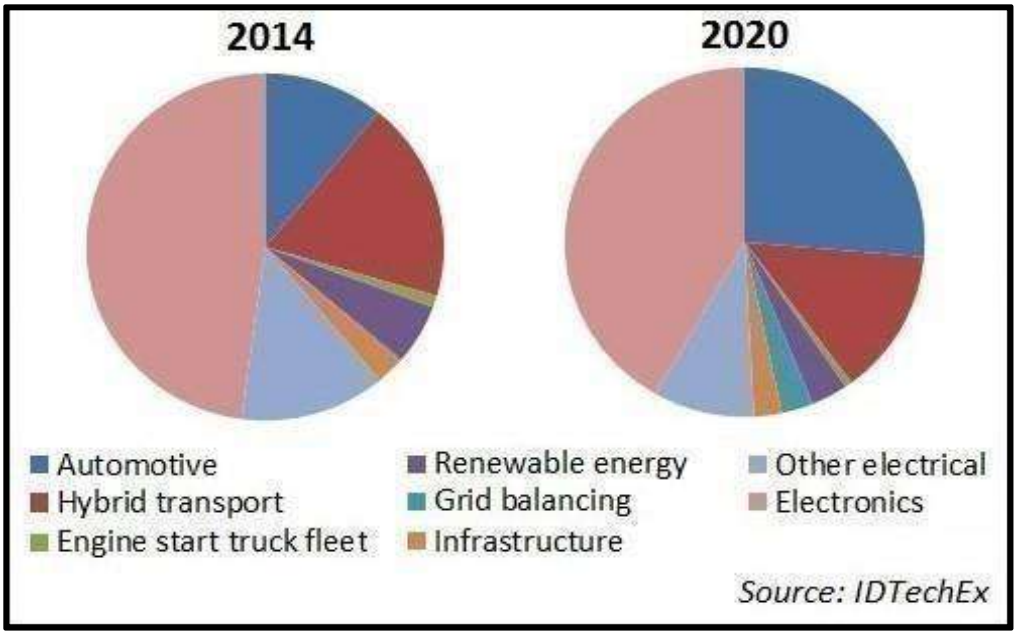

Figure 5. Supercapacitor global market applications in the year 2014 and 2020 [13]

1.4.1 Limitations of Supercapacitors

The Ragone plot for various energy storage systems is shown in Figure 5. The main drawback of EDLC is that it has a lower specific energy than batteries. Supercapacitors currently achieve specific energy levels of only 5-10Whkg^{-1} [14, 15], which is 3 to 15 times less than that of batteries. Various efforts are made to increase the energy density of supercapacitors in order to realize their potential in a variety of applications. The electrochemical stability window (ESW) of an electrolyte determines how much energy a supercapacitor can store.

A higher ESW electrolyte, such as an organic electrolyte (2.5V) or an ionic liquid (3.5V), is being used to replace the electrolyte in supercapacitors as they are currently being developed [16, 17]. In addition, various other forms of carbon, including graphene, carbon nanotubes, carbon derived from carbides, and carbon aerogel, are also investigated for their potential as an electrode material for energy storage systems. However, the majority of systems are constrained by expensive production costs and challenges with mass production to meet commercial market demand [18].

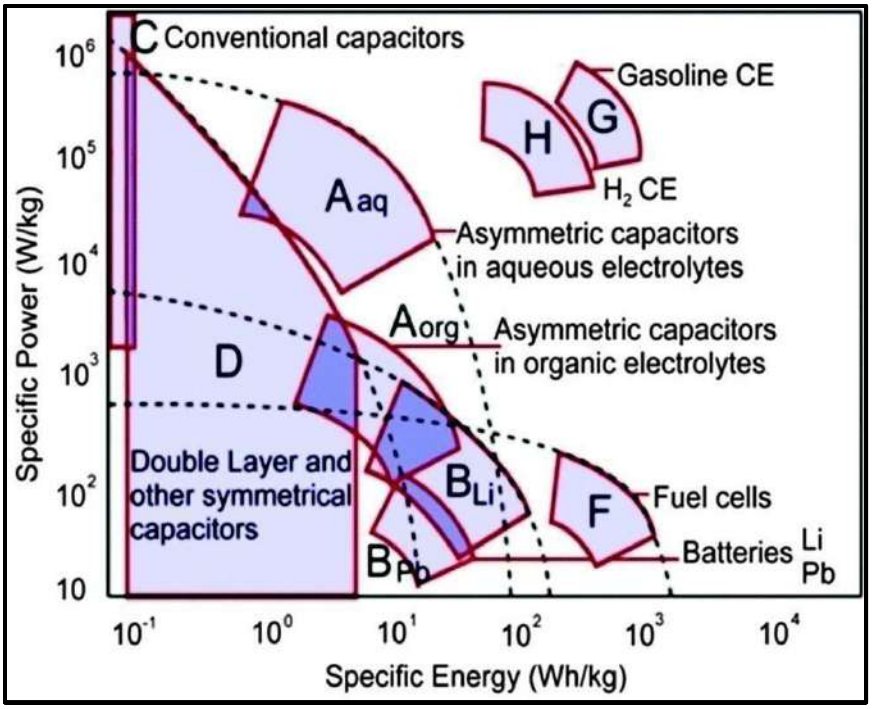

Figure 6. Ragone plot (specific power against specific energy) for various energy storage devices [19]

According to the supercapacitor's energy storage mechanism, the specific surface area of activated carbon has a significant impact on the device's capacitance (AC). However, there are numerous carbon activation techniques to increase the surface area of AC. The majority of recently reported activated carbons made from biomass are currently prepared through chemical activation in order to increase surface area [20]. With chemical activation, however, irregular morphology and structure of AC were seen [21]. Chemical activation also results in AC surface doping, which makes it difficult to comprehend the actual charging and dischargingprocess of supercapacitors. The post-process to remove the excess chemical from the AC also comes at an additional cost. As a result of their disposal, some chemicals, like phosphoric acid or zinc salt, may cause secondary environmental pollution [22].

Nowadays, ACs are typically produced for a reasonable price. A high-performance AC has a production cost that is roughly half that of a supercapacitor [23]. Thus, one of the goals to satisfy the enormous market demand in the future is to reduce the cost of producing high-performance AC for supercapacitor applications. The preparation of AC from waste biomass as electrode materials for supercapacitor applications has recently attracted research attention and has demonstrated performance that is comparable to that of commercial supercapacitors.

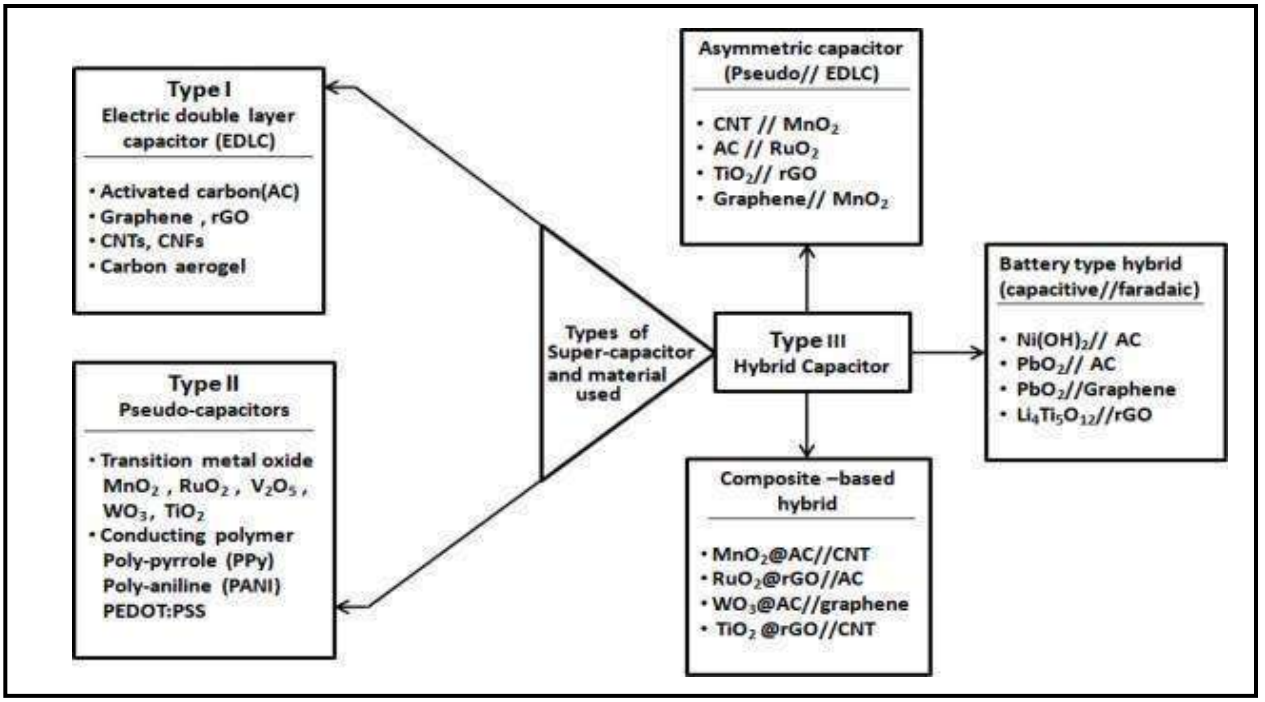

Figure 7. Types of Supercapacitors and used material

CHAPTER 2

Literature Review

The first part of this chapter focuses on the working principle of an EDLC, its configuration, and typical performance assessments for an EDLC. This section reviews the electrolytes and electrode materials as significant determinants of an EDLC's electrochemical performance. The most often used active component in an EDLC electrode is activated carbon. Physical and chemical activation methods, which are both often employed to prepare ACs from biomass utilized as carbon precursors, are covered.

2.1 Working Principle & Properties of Supercapacitor

High-power electrochemical energy storage systems are known as supercapacitors, electrochemical double-layer capacitors (EDLCs), or ultracapacitors. Due to the enormous surface area of the active material in electrodes, supercapacitors have a substantially higher storage capacity and energy density than regular capacitors. Although a supercapacitor's structure is relatively similar to that of a battery, it differs from a battery in that supercapacitors store energy electrostatically on the surface of the active material without using a redox reaction. Additionally, as EDLC performs charging and discharging through simple ion adsorption and release without needing any redox reaction, EDLCs offer higher charge-discharge rates (60-120 s). Additionally, EDLCs have great cyclability (10^6 cycles), increased power density (more than 1000-1500 $W.kg^{-1}$), and high cycling efficiency (98%) [24].

An EDLC is made up of two high surface area porous electrodes that are separated by a porous separator and submerged in an electrolyte. Supercapacitor electrodes are often a blend of high conductivity materials and AC with a polymer binder. In order to increase the conductivity of electrodes with no more than 5% mass, carbon black (CB) is frequently employed as an addition [25].

In the supercapacitor electrode, polymer binders such as polyvinylidene fluoride (PVDF), polytetrafluoroethylene (PTFE), or nafion are frequently used. To prevent self-discharge and any chemical reactions with the electrolyte while maintaining good ionic conductivity and ion mobility during the charge and discharge process, the separator must be carefully chosen [26]. To conduct the electrical current from each electrode in an EDLC, current collectors are crucial. As current collectors for the energy storage system, metal foil or polymer-coated carbon can be utilized [27]. Due to its affordability, toughness, and stability in organic and ionic-liquid based (IL) electrolyte, aluminium is a frequently utilized metal as the current collector for EDLC. Other metal current

collectors are also readily available, including nickel foils [28], copper, platinum, and stainless steel. The strong chemical resistivity and electrolyte-corrosion resistance of the current collector are the determining factors in its choice for EDLC.

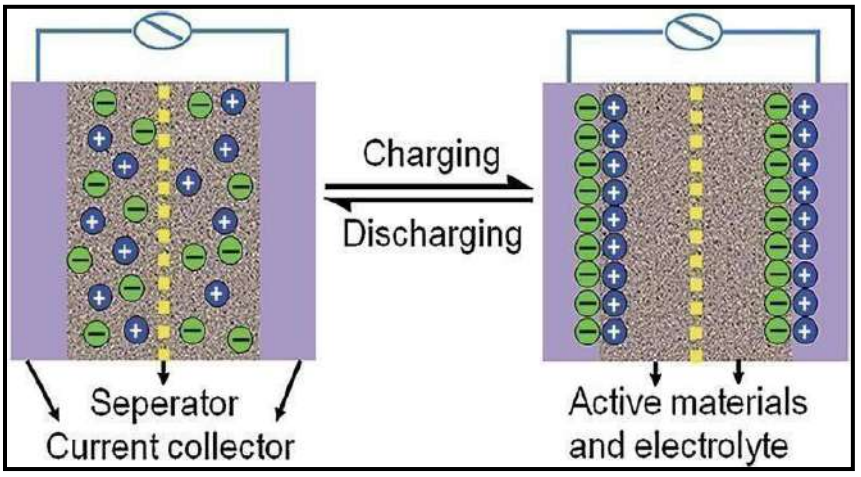

Figure 8. Charge storage mechanism of EDLC

When voltage is applied across an EDLC's porous electrodes, the positive electrode draws electrolyte ions of the opposing sign, which cause charges to build up on the electrode's surface. Meanwhile, the negative electrode draws positive electrolyte ions, beginning the charging process. When the discharging process takes place, the EDLC releases energy. A pure EDLC typically stores energy based on electric double-layer capacitance from charge accumulation on both electrode surfaces without any charge transfer between the electrolyte and electrode interface.

A supercapacitor, also known as a pseudo-capacitor, can store energy in addition to having an electric double layer characteristic by quickly reversible redox reactions occurring on the electrode surface. When functional groups on the carbon electrode interact chemically and electrochemically with the cell's electrolyte, pseudo-capacitance results [29]. By combining this effect with the EDL capacitance, the specific capacitance of a supercapacitor can be further increased. The pseudo-capacitance will show a strong peak at specific voltage values when the enthalpy of ion-electrode interactions deviates slightly from its average value. The redox charging process is identifiable by the prominent peaks (redox peaks) in cyclic voltammetry (CV) curves. The quick reversibility of the reactions and lack of any phase change in the electrode molecules or chemical bond distinguishes the faradaic reaction in supercapacitors from that in batteries.

The attachment of the de-solvated ions (redox ions) to the same charged electrode surface causes the pseudo effect (shown in Figure 9). Additionally, there are ion pairs that exist in the solvent (solvated ions) that may prevent ions from diffusing onto the electrode surface in capacitor

devices [30].

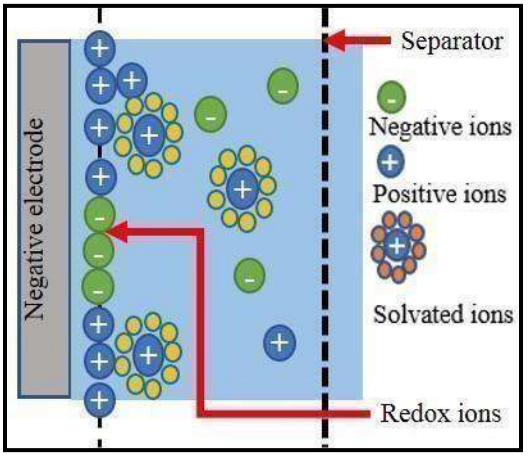

Figure 9. Simplified diagram of a double layer with redox ions causes the faradaic charge-transfer of the pseudo-capacitance.

2.1.1 The Double Layer Mechanism

The interfacial area between the electrolyte ions and the electrode determines how much energy may be stored in EDLCs according to the electric double layer mechanism.

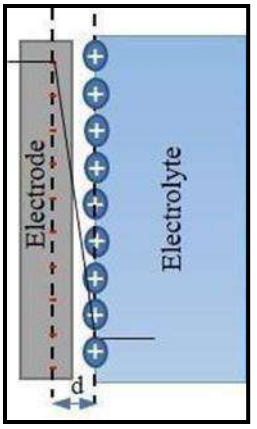

Figure 10. The Helmholtz layer

In the pores on the surface of the active materials, the electrolyte ions disperse throughout the separator and adhere to them. To improve energy storage, electrode materials with high surface areas and suitable pore sizes that match the size of the electrolyte's ions are crucial [31, 32].

2.1.2 Models of EDLCs

There are three models that are used to describe the behavior in EDLCs;

(a) the Helmholtz model,

(b) the Gouy-Chapman model and

(c) the Stern model.

The Helmholtz model, which depends on the concentration of the electrolyte and the size of the ion, represents the double layer effect as two surfaces with opposite charges that are separated by a little distance (Figure 9) [33].

The Gouy-Chapman model expanded on the Helmholtz model by taking into account the ion charge distribution caused by thermal motion, sometimes known as a diffuse layer (Figure 10). The performance of highly charged EDLCs, however, was overestimated by the Gouy-Chapman model. The diffusion layer (CD) and the capacitive contribution of the Helmholtz layer (CH), which combine the Helmholtz model with the Gouy-Chapman model, are two distinct regions of ion distributions that were included in Stern's model.

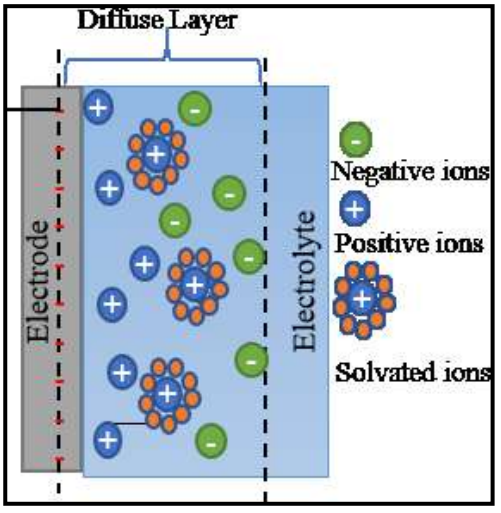

Figure 11. The Stern model

2.2 Two-electrode vs Three-electrode EDLC

To assess EDLC performance, symmetrical two or three-electrode cells are frequently used together. A working electrode (WE), a counter electrode (CE), and a reference electrode (RE) are the three electrodes that make up a three-electrode cell, which is typically manufactured for researchpurposes [34]. The WE is typically coated with active substances like activated carbon or another type of carbon that is being researched. A CE is an electrode that measures the WE's potential without getting involved in the cell's electrochemical process. It is typically constructed of inert

substances such glassy carbon, platinum, or gold. In order to prevent it from becoming the limiting factor in the kinetics of the electrochemical reaction as the current flows between the WE and the CE, a CE's total surface is higher than a WE's. While the WE is used to assess the potential of the working electrode without passing current through, the RE is utilized to provide a stable potential for controlled regulation of the working electrode.

Different capacitance values may result from how three-electrode and two-electrode cells are configured. Three-electrode cell capacitance measurements are typically greater than those for actual two-electrode devices [35].

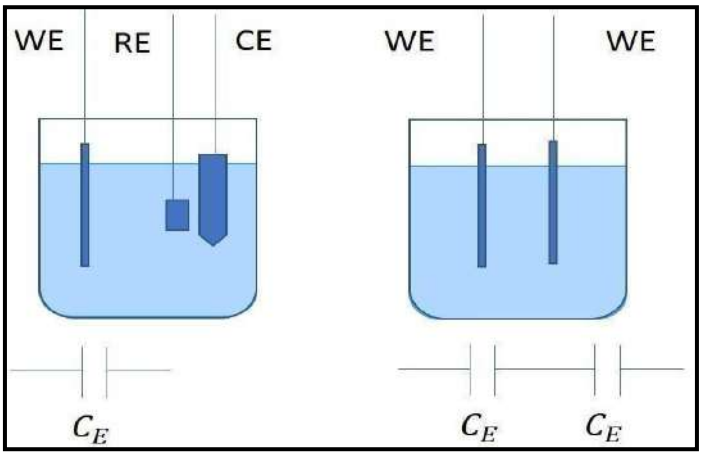

Figure 12. Schematic view of (a) Three-electrode and (b) two-electrode cell setup.

The working electrode (WE), Reference Electrode (RE) and Counter electrode (CE)

Despite the lower capacitance value, the measurement of two- electrode cells more accurately capture the functionality of EDLCs in actual use [36]. Figure 12 depicts a two-electrode cell with two symmetrical functioning electrodes.

Suppose the mass of active electrode material as *m*, the capacitance of a single electrode (CE) is equal to the specific capacitance (C_{3e}) of the three-electrode cell, which can be calculated by dividing by the mass of active electrode material as shown in Equation 1.

$$C_{3e} = C_E / m \qquad \textbf{Equation 1}$$

For a symmetrical two-electrode cell, which is equivalent to a practical EDLC, the total capacitance (C_{t2e}) can be obtained using Equation 2.

$$C_{t2e} = 1 / C_E + 1 / C_E \qquad \textbf{Equation 2}$$

Since the mass from each electrode in the symmetrical two-electrode cell is equal, the relationship of the capacitance from the two-electrode cell and a single electrode in the measured

three-electrode as in Equation 3.

$$1/C_{t2e} = 2/C_E \quad \textbf{Equation 3}$$

By considering the specific capacitance of each electrode is identical, thus the specific capacitance (C_{2e}) of two-electrode cells as Equation 4.

$$C_{2e} = C_{2e}/2m = C_E/4m \quad \textbf{Equation 4}$$

In this work, two-electrode EDLC was also assembled to reflect the efficiency of material as a real commercial device.

2.3 The performance evaluation of EDLCs

Generally, the performance of an EDLC can be determined based on

(a) the capacitance,

(b) the power density,

(c) the energy density

(d) the cyclic stability,

(e) the equivalent series resistance (ESR) of the cell

An EDLC's capacitance is its capacity to store energy by building up electric charges on its surface and electrodes. Equation 5 can be used to calculate the capacitance, where C stands for capacitance (Farads), Q for charge (Coulombs), and V for voltage (Volts).

$$C = Q/V \quad \textbf{Equation 5}$$

A high ESR value indicates that the cell has a high internal resistance (IR), which lowers performance by manifesting as a high IR drop, noise, or high potential drop. The most popular technique for determining the ESR is the IR drop from the GC test discharge curve [27]. By applying Ohm's law, the ESR can be determined using Equation 6.

$$R_{ESR} = \Delta V/\Delta I \quad \textbf{Equation 6}$$

The performance parameters of an EDLC can be assessed using a variety of techniques in both research and industry. Cyclic voltammetry (CV), galvanostatic charge and discharge (GCD), and electrochemical impedance spectroscopy (EIS) are three of the evaluation techniques that are frequently used to assess EDLC performance. Three fundamental factors can be used to compute the equivalent series resistance (ESR), power and energy densities, and capacitance of an EDLC (potential, current and time).

2.3 Electrolytes

The capacitance of the EDLC is significantly influenced by the type of electrolyte used in the cell. Electrochemical stability windows differ depending on the kind of electrolyte (ESW). The electrolyte's ESW is the potential range in which an EDLC can function without its electrolyte oxidizing or decomposing.

An electrolyte with a wider ESW hence produces more energy density. The choice of the electrolyte also has a significant impact on other EDLC characteristics such internal resistance, rate of energy release, operating temperature range, and cyclic stability [37]. The thermal stability and operating temperature range of EDLCs can be significantly impacted by the solubility and viscosity of the electrolyte. Aqueous electrolytes, organic electrolytes, and ionic liquids are the three main types of liquid electrolytes used in EDLC applications.

Ion size and the compatibility between pore size and ion size are additional elements that can have an impact on the performance of an EDLC in addition to the ESW of the electrolytes [37]. There are, however, few studies that examine the relationships between the effectiveness of EDLC and the pore size of the electrode materials in various electrolyte systems. According to Zeller et al. [38], the electrolytes utilized affect how much the effective surface area contributes to an EDLC's capacitance. The specific surface area of the electrode materials in the acid-based electrolyte system determines the capacitance of the EDLC. While with an organic-based system the capacitance is only dependent on the exterior surface area. The results go against Zhou et al. [39] claimed, according to which the specific surface area and high meso-porosity of activated carbon inorganic electrolyte-based supercapacitors affect the specific capacitance.

2.3.1 Aqueous Electrolytes

Acidic, alkaline, and neutral electrolytes are different types of aqueous electrolytes. KOH [40–45] and H_2SO_4 [45–49] are the electrolytes that are most frequently employed for EDLC research among all other electrolytes in published literature. Due to their high conductivity, low cost, thermal stability, and simplicity of assembly in the atmosphere, aqueous electrolytes are appealing.

Compared to organic and IL electrolytes, aqueous electrolytes have a high conductivity. While organic electrolyte $TEABF_4$ /PC only displays ionic conductivity of 0.02 Scm^{-1} [51], the ionic conductivity of 30% H_2SO_4 electrolyte reaches a high value up to 1 Scm^{-1} [50]. In an EDLC, the increased ionic conductivity of the electrolyte results in a reduced equivalent series resistance (ESR), which enhances power density and allows for quicker charge and discharge stages [29]. The narrow ESW (1.299V) causes the operating voltage of an aqueous-based EDLCs to be comparatively low (1V) [40]. Additionally, the aqueous electrolyte is readily electrolyzed to produce gases that might

lead to issues like swelling. In order to prevent corrosion issues in the cell caused by the use of acid electrolytes, it is required to employ cell components composed of gold or platinum. Additionally, the operational temperature ranges are constrained to the freezing and boiling points of water.

There have been a number of reported attempts to increase the ESW of aqueous electrolytes. By using the constant current technique, the ESW for an aqueous electrolyte containing 5 M $LiNO_3$ was increased to 2.3V [52]. The combination of carbon nanotubes with MnO_2 has led to an ESW of 2V for KNO_3 as a consequence of research into various electrode materials to improve the ESW of an aqueous solution.

Although it is still below the ESW of commercially available organic electrolytes (2.5-2.7V), the maximal ESW is still constrained at roughly 2V [54]. As of right now, the largest ESW of 3.2V was reported utilizing a saturated sodium perchlorate aqueous electrolyte without emitting any gases [53].

2.3.2 Organic Electrolytes

The non-aqueous electrolyte is another name for the organic electrolyte. Organic electrolytes are less expensive than aqueous electrolytes since they are compatible with the aluminium components of a cell. Although compared to aqueous solutions, organic electrolytes are less conductive, more expensive, and require a more involved assembly process, the majority of commercially available supercapacitors use an organic-based electrolyte with a larger ESW [55]. Acetonitrile (ACN) or propylene carbonate (PC) are typically used as solvents with organic electrolytes in the ESW range of 2.5-2.7V in commercial EDLCs [37]. Despite ACN having a substantially lower internal resistance than PC, PC is the preferred organic electrolyte for use [36]. According to Table 1, at a temperature of 25 ºC, ACN has a viscosity that is significantly lower than PC (0.3 mPa/s vs. 2.5 mPa/s). ACN has significant toxicity and flammability issues, though. As a result, PC has been thought of as a safer option to ACN. The water content must be kept below 5 ppm in order to operateat the maximum ESW of electrolyte [56].

Table 1. Physical properties of PC and ACN with 0.65 M of $TEABF_4$ at 25 ºC [37]

Type of solvent	Relative permittivity	Viscosity (cp)	Boiling point (ºC)	Melting point (ºC)	Molecular weight	Ionic conductivity ($mScm^{-1}$)
PC	65	2.5	242	-49	102	10.6
ACN	36	0.3	82	-49	41	49.6

Generally, the aqueous-based EDLCs have higher specific capacitance than organic-based electrolytes [38, 57]. For organic electrolytes, cation and anion sizes are bigger than for aqueous electrolytes [37]. This may reduce the amount of electrolyte ions that can diffuse through carbon

materials with pores smaller than their size. Therefore, to increase the specific capacitance of an EDLC, it is crucial to have a pore size that is compatible with the electrolyte ions.

2.3.3 Ionic Liquids

The ionic liquids (IL) having a low melting point under 100 °C are molten at room temperature [58]. Typically, high asymmetric sized cations and anions make up an IL. Through the modification of the substituent groups or the cation/anion pair, this special combination enables ILs to fine-tune their physical and chemical properties [59–61]. ILs have drawn a lot of interest as alternate electrolytes for EDLC because of their distinctive characteristics [62–64]. The features of strong thermal and chemical stability, non-flammability, and minor volatility are further benefits of ILs [35, 36]. Since IL-based EDLCs have a broader ESW (3.5-4V) than all other types of electrolytes available for EDLCs, they have been found to have higher power and energy densities than organic and aqueous-based EDLCs [65].

However, the high viscosities and relatively low ionic conductivities of ILs ($0.01 scm^{-1}$) [66] prevent their practical application in commercial EDLC markets. As shown in Table 2, the ionic conductivity of $EMIMBF_4$ is relatively high at 14 $mScm^{-1}$. In contrast to the conductivity of organic electrolytes listed in Table 1, this is still significantly less. Additionally, the viscosity of $EMIMBF_4$ [55] is significantly larger than that of organic electrolytes based on PC or ACN, each of which has a viscosity of 0.3 cp (Table 1).

Due to its low melting point of slightly over 273 K, ILs may be difficult to operate at low temperatures. It is crucial to research how the size of the carbon electrode matches up with the size of the ions in the electrolytes since at different temperatures, ILs contain varying lengths of hydrocarbon chains and cations as well as varying sizes of solvated and un-solvated ions [67]. Additionally, ILs are far more expensive than organic electrolytes and require a complex handling process to guarantee there is no water present.

Table 2. Physical properties of $EMIMBF_4$, IL at 25 °C

Type of solvent	**Relative permittivity [68]**	**viscosity (cp) [67]**	**Boiling Point (°C)**	**Melting point (°C)**	**Molecular weight**	**Ionic conductivity ($mScm^{-1}$)[69]**
$EMIMBF_4$	13.9±0.4	41	>350	15	197.97	14.1

2.4 Electrode Materials

The parameters of the electrode material employed have a significant impact on the capacitance and energy storage of an EDLC. The specific surface area of the electrode has a significant impact on a cell's capacitance, according to the double layer mechanism of EDLCs. The specific surface area of the electrode materials does not, however, directly correlate with the observed capacitance [62, 64]. The capacitance in EDLC is not entirely caused by the surface area of the electrode materials. If the carbon material's pores are smaller than the electrolyte ions and prevent the electrolyte ions from being accessible [64]. The double layer capacitance is significantly increased by matching the pore size of the electrode materials with the electrolyte ions [37]. Additionally, it has been discovered that the functional groups on the carbon surface improve the wettability of materials and produce the Faradaic effect, which is advantageous for EDLC performance [72]. In order to increase the capacitance of EDLCs, different attempts have been made to develop novel electrode materials.

For EDLC and pseudo-capacitor applications, electrode materials fall into one of three main categories:

(a) carbon-based,

(b) conductive polymer, or

(c) metal oxides.

Conductive polymer and metal oxide materials, which support charge storage and involve reversible surface redox reaction, are regarded as Faradaic materials [70].

Table 3. An overview of electrode materials for EDLC and Pseudo-capacitor

EDLC	**Pseudo-capacitor**
Activated carbon (AC) [12, 73-75]	Conductive polymers [80]
Graphene [76, 77]	Metal oxides [81]
Carbon nanotubes (CNT) [78]	Metal hydroxides [82]
Carbide-derived carbon, Carbon aerogels [79]	Functionalized carbon [83, 84]

2.4.1 Activated Carbon

AC with a large surface area is frequently employed in industries for applications like air and water purification, food and beverage production, pharmaceutical development, and catalytic activity [85]. Coconut shells are used almost exclusively as precursors in the manufacturing of AC for

supercapacitors. One of the best strategies to lessen the environmental impact of the disposal of biomass wastes is to convert the waste into high-value items like AC with large surfaces.

Based on various experimental settings, physical activation and chemical activation are typically the common active techniques to convert biomass to activated carbon. Chemical activation can be used in either a one or two step technique to prepare AC. For the traditional physical activation approach, pyrolysis or carbonization is followed by activation to prepare AC in a two-step process.

2.4.2 Carbonization

By pyrolyzing organic compounds without oxygen, carbonization is a thermal degradation process that produces residues that are rich in carbon. The process results in the carbon-rich byproducts known as char, bio-oil, and flammable gases. Before physical activation, the excess moisture and volatiles in the biomass must be removed through carbonization. The energy required to dissolve the chemical bonds in the biomass and create the basic carbon structure as well as the porosity on the char is related to the carbonization temperature [86].

To regulate the yield and composition of the carbonized samples, many investigations have focused on the carbonization temperature and heating rate [87]. According to a study, char made from rice straw has reduced surface area when it is heated at a high rate and at a temperature of 900°C [88]. The specific surface area of the char increases from 398 to 555 $m^2.g^{-1}$ when the heating rate of oil palm frond fibre is decreased from 30 to 10 °C min^{-1}, according to a similar observation. The surface area and pore volume of char made from eucalyptus, in contrast, were found to increase with the pace of heating. According to Cetin et al. [89], a high heating rate caused the char to become reactive, which resulted in increased porosity forming. Despite numerous studies on the impact of heating rate, the structure and porosity of the char generation remain inconsistently understood.

2.4.3 Activation

By removing disordered regions and blockages caused by degraded volatile, the activation process generates and improves the porosity of char. However, the characteristics of the precursors, the carbonization conditions, and the choice of activation method all affect the activated carbon's increase in porosity and surface area [37]. When making activated carbon, a variety of techniques are used, including physical, chemical, physiochemical (a combination of chemical and physical activation), and microwave-induced activation.

2.4.3.1 Chemical activation

To increase the surface area and pore volume of ACs, chemical activation is used. Chemical active agents used in this process include phosphoric acid (H3PO4), zinc chloride ($ZnCl_2$), sodium hydroxide (NaOH), potassium carbonate (K_2CO_3), ferric chloride ($FeCl_3$), and potassium hydroxide

(KOH) [90]. The majority of chemical activation processes are one-step procedures, allowing for simultaneous activation and removal of volatiles at a relatively low temperature in a single step. The chemical works as a dehydrating or oxidizing agent during the activation process to speed up the pyrolytic decomposition and lessen the creation of volatile compounds, which causes charring and the formation of the porous structure. In comparison to those created through physical activation, activated carbons (ACs) prepared chemically exhibit greater specific surface areas, a better porous structure, and higher yields [91]. KOH is the most widely used chemical activating agent out of all the others. High specific surface area and a clearly defined pore size distribution are produced by KOH activation in AC [92]. Researchers still could not fully comprehend the precise activation mechanism of KOH activation, though.

The chemical activation procedure has several other drawbacks as well, such as the corrosiveness. Harsh chemicals can alter the structure and morphology, and chemical activation results in surface doping and additional functional groups [93]. To eliminate surplus activating agent, additional washing stage is required following the chemical activation process, which raises the cost of producing electrode materials. As a result of their disposal, some chemicals, such as phosphoric acids or zinc salts, may cause secondary environmental pollution [94].

2.4.3.2 Physical activation

Physical activation often involves a two-step procedure. In order to create activated carbon, raw materials must first undergo carbonization to remove volatile components of the biomass. This is followed by activation at a high temperature in the presence of an oxidizing agent, such as carbon dioxide (CO_2), steam, or air, which increases porosity and surface area. It is a highly endothermic reaction that uses CO_2 to activate carbon in order to create carbon monoxide when reacting with carbon. the carbon monoxide that results from the CO_2.

To develop carbon's porosity, the activation method causes a gasification reaction. High temperature helps an oxidizing agent enter the char's interior structure and remove additional carbon atoms during the gasification process, which causes the pores that are inaccessible to be opened and widened [94].

CHAPTER 3

Materials & Methodology

3.1 Study Design

The research will be analytical in nature.

3.2 Sample Collection

Clean maize cobs blocks and pieces of wood waste used in this study were collected from Punjab region, capital city of Pakistan 'Islamabad'.

3.3 Required Chemicals

- Potassium Hydroxide (KOH)
- Hydrogen Chloride (HCl)
- Nafion
- Ethanol

3.4 Sample Preparation

3.4.1 Materials

Clean maize cobs blocks and pieces of wood waste used in this study were collected from a local market (Islamabad, Pakistan). Potassium hydroxide (KOH), hydrochloric acid (HCl), ethanol and deionized (DI) water were obtained from Sigma Aldrich (Czech Republic). Few µl of Nafion was used. All chemicals and reagents are of analytical grade and have been used as such with no more purification.

3.4.1.1 Preparation of pyrolyzed simple carbon materials (SC-C & SC-W)

Mechanically treated maize cobs had their inner pith removed. For the manufacture of carbon materials, hardwood outer rings were employed for the study. These hardwood ring blocks and wood pieces were further chopped into tiny pieces for the pyrolysis procedure. These maize cob and wood chunks were pyrolyzed (or carbonized) for two hours at 700°C in a Protherm tube furnace under an argon atmosphere (Ar). The system was then allowed to cool down to ambient temperature while being continuously supplied with Ar gas. The so- produced charcoal samples were referred to as simple carbon of maize cob and wood scraps (SC-C, SC- W).

3.4.1.2 Preparation of pyrolyzed KOH-activated carbon materials (AC-C & AC-W)

For the activation procedure, these prepared simple carbons made from maize cob and wood waste were further ground in a ceramic mortar. The solution was then prepared in terms of a 4:1:1 ratio, 800 mg of potassium hydroxide (KOH), 200 mg of simple maize cob, had been

dissolved on 80 mL of ethanol. In a separate beaker, the same suspension was made for wood pieces by combining 800 mg of KOH with 80 mL of ethanol and 200 mg of the simple carbon (in terms of 4:1:1 ratio).

The resulting suspension liquids were stirred for four to five hours at room temperature. Following proper drying at 60 degrees Celsius for 24 hours in a vacuum oven, the produced KOH activated suspension was dried by hot plate to evaporate the solvent (ethanol). These obtained activated carbons of maize cob and wood pieces were denoted as AC-C, AC-W. Additionally, the AC-C and AC-W were annealed in a Protherm tube furnace for two hours at 700°C under argon atmosphere (Ar). Later, the system was allowed to drop down to room temperature with the continual flow of Ar gas.

3.4.1.3 Washing/Centrifugation of prepared KOH-activated carbon materials

The obtained samples of activated carbons (AC-C, AC-W) were then dried at 60 °C for 24 hours in a vacuum oven. Then, these prepared samples were washed many times with 3 M HCl and deionized water (DI water) to eliminate the contaminants. Hierarchical porous pyrolyzed KOH- activated carbons (AC-C, AC-W) were successfully produced as a result.

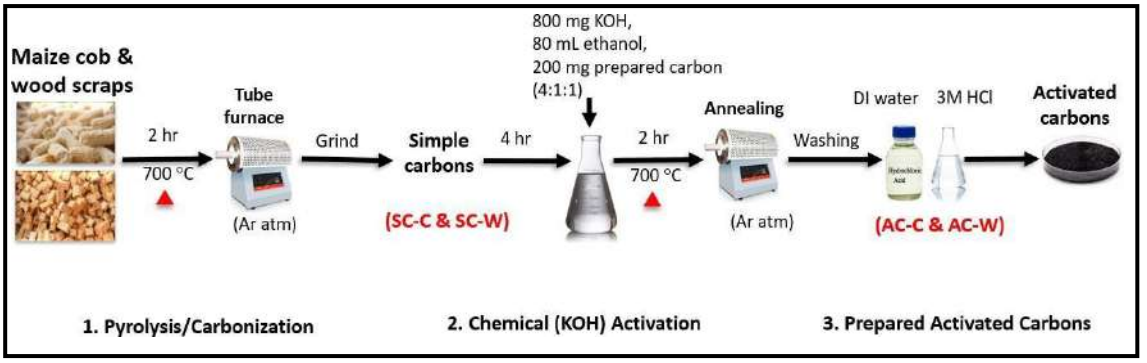

Figure 13. Schematic illustration of preparation of simple carbon & activated carbons of selected biowastes (SC-C, SC-W, AC-C, AC-W)

3.4.1.4 Preparation of Supercapacitor electrode

To make the supercapacitor electrode of corn cob, 1 mg AC-C, 10 µL Nafion, and 1 mL ethanol was added into an Eppendorf to prepare homogenous suspensions (slurry prepared). Respectively, slurry for electrode of wood waste (AC-W) was prepared in another Eppendorf. The as-obtained mixed slurry was deposited on glassy carbon electrode, which was employed as a current collector for further electrochemical characterization, after ultrasound and stirring treatment.

3.4.1.5 Preparation of KOH electrolyte

To prepare 6M KOH electrolyte, 33.66 grams of KOH was measured and added into a beaker

with 66 ml DI water. The prepared 6M KOH electrolyte was used for three and two-electrode testing where CV (cyclic voltammetry), GCD (galvanostatic charge-discharge), EIS (electrochemical impedance spectroscopy) and cycle stability was done.

3.4.1.6 Characterizations of prepared materials

The material's crystallographic and composition information was studied using X-ray diffraction (XRD, Hong Kong, China). The morphology of all prepared carbon materials (SC-C, SC-W, AC-C, AC-W) was studied using scanning electron microscopy (SEM, JSM 6490A, JEOL, Japan) and equipped with an energy dispersive X-ray spectroscope (EDX), Shanghai, China) to study the elemental composition. Moreover, the pyrolysis process (TGA, TA Instruments, SDT Q600, Shanghai, China) was studied using thermogravimetric analysis from room temperature to 700°C with a temperature rise of 5°C per min and a nitrogen flow of 10 sccm. Fourier transform infrared (FTIR) spectra were carried out using a Thermo Scientific Nicolet iS5 with wavelength range from 4000 to 400 cm^{-1} to study the chemical composition of prepared materials. Raman spectroscopy was used to evaluate the degree of functionalization before and activation of all the prepared samples.

3.4.1.7 Electrochemical Characterization

The electrochemical characteristics of the as-obtained carbon materials were investigated in a three- electrode setup employing them as a single electrode. The working electrode was the glassy carbon electrode (GCE) coated with as-prepared slurry and left to dry it at room temperature, the counter electrode was the platinum foil, and the used reference electrode was the mercury electrode (Hg/HgO), respectively.

In order to evaluate the electrochemical characteristics i. e. CV, GCD, EIS, cycle stability of the AC-C, AC-W, a CHI 760E (CH Instrument, Texas, USA) an electrochemical workstation was used. Cyclic Voltametric (CV) analysis was done over a voltage span of 0V-0.6V in a 6 M KOH electrolyte at diverse scan rates ranging from 10 to 100 m V/s including 15, 20, 30, 50, 80, and 100 m V/s. The galvanostatic charge/discharge analysis was done at different current densities i. e. 1, 2, 3, 5, 8, 10 A/g. Electrochemical impedance spectroscopy (EIS) was done by above electrochemical operating station at a frequency of 1 Hz to 100 Hz in 6 M KOH electrolyte. The 6 M KOH solution was used as an electrolyte for all the tests mentioned above.

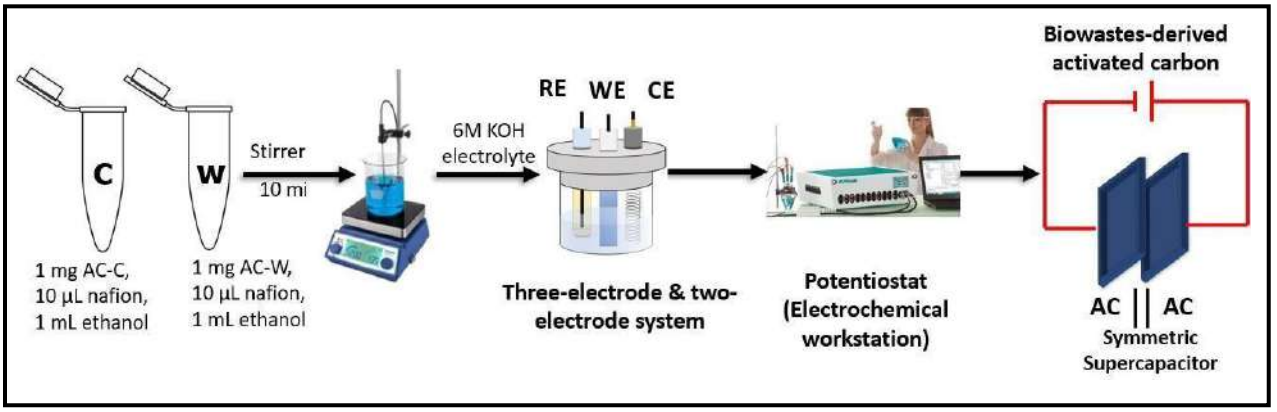

Figure 14. Schematic illustration of preparation of supercapacitor electrodes & electrochemical characterization of prepared electrodes

Specific capacitances for GCD testing were measured as follows:

- $C_S = it / m.\Delta V$ **Equation 7**

Where, Cs is the specific capacitance (Fg^{-2}),

i is the current (A),

t is the discharge time (s),

m is the mass of the electrode material (g) and

ΔV is the potential window (V)

Energy and power densities are calculated based on the following equations:

- $E = C_S / 2\Delta V^2$ **Equation 8**
- $P = E / t$ **Equation 9**

Where, E is the energy density ($Whkg^{-1}$) and P is the power density (Wkg^{-1}).

CHAPTER 4

Results and Discussion

4.1 Structure analysis

The goal was to combine the numerous channels and pores found in selected biowastes with the additional pores created during the pyrolysis/carbonization and activation processes of hierarchically porous structure of pyrolyzed activated carbons. Pore diameters of the materials are predicted to be covered by following the simple, eco-friendly and cost-effective two step method. Different scales of pores diameter such as macroscopic macropores (10μm-100nm), dispersed mesopores (50-10nm), and abundant micropores (< 2nm) were encountered and explained in a later section [95]. Electrolyte ions were transported and diffused efficiently through pores of the appropriate size. Although macropores have a minor effect on capacitance, they may operate as a 'reservoir' for the electrolyte. As it allows electrolyte to reach the electrode surface fast. While micropores may increase the electrode's SSA, as a result increase the contact area between the electrolyte and the electrode and it favors the electrochemical capacitance. But when the micropore volume was exceeded, however, the ion conduction resistance from the electrolyte to the carbon surface raised, results in a loss in capacitance. Surprisingly, presence of meso-pores, especially when the diameter was >3 nm, promoted fast electrolyte ion diffusion and provided enough electrolyte ion transport [96-99].

The hardness of corn cob and wood chunks used in the study is primarily made up of cellulose, as well as several additional components such as hemicellulose and lignin [96]. Carbon compounds with macro and meso holes inherited from natural biowaste sources are generated through pyrolysis in a tubular furnace. Active sites and amorphous carbon on the inner wall of the tracheid were oxidized by CO_2, so that the blocked pores were opened, the original pores were further enlarged and some new pores were created. Then the pores were created on the tracheid wall by KOH activation, which strongly etched the tracheid wall of the carbon material to create more micropores and nanopores. The introduction of surface oxygen groups on the carbon samples treated by acid- KOH facilitates sufficient contact between the electrode material and the electrolyte. Mechanisms of KOH activation based on activated carbon have been addressed [100]. The reaction of carbon and KOH starts as;

$$\mathbf{6\ KOH + 2\ C \rightarrow 2\ K_2CO_3 + 2\ K + 3\ H_2}$$

Finally, a hierarchical porosity is formed as a result of the high specific surface area (SSA).

4.1.1 Morphology and structural properties of electrode materials

The material characteristics of biowastes-derived all carbon materials (SC-C, SC-W, AC-C, AC-W) was investigated using Raman spectroscopy, TGA, SEM, XRD, BET, and FTIR tests.

4.1.1.1 Scanning Electron Microscopy (SEM) & Elemental Dispersive X-Ray (EDX) The hierarchical porosity (microstructure) of prepared carbon materials is systemically verifiedby SEM images. It can be seen that the morphologies and porosity of these carbons are strongly dependent on the pyrolysis temperature and activation process. The samples SC-C, SC-W (Figure 3 (b, d)) show a relatively smooth surface with large numbers of macropores over which a small number of etched pores were observed. Whereas, in comparison to SC-C, SC-W images; the SEM images of AC-C, AC-W (Figure 3 (a, d)) clearly confirms the formation of micro-size pores (micropores) and mesopores throughout the sample that might act as an ion buffer pool and could significantly reduce the electrolyte-ion diffusion distance in the device. Two facts can be derived from the observations are: 1) the mild KOH soaking, togetherwith the one-step carbonization procedure, can effectively create porosity in the corncob and wood carbon materials; 2) the degree of porosity can be readily controlled by the KOH soaking time. Additionally, at the nano-scale, porous tunnel structures can be observed in the activated carbons, which may result from etching of the carbon framework or the gasification of CO_2 evolved from K_2CO_3 [101]. The above observation clearly confirmed that KOH activation of carbon results the formation of pores over the carbon materials. These abundant meso and micropores contribute to a high surface area and prior capacitance behaviors [102].

The EDX data indicates that all the prepared samples are composed of carbon, oxygen, and nitrogen (Table 4). EDX data confirms that the AC-C and AC-W has 80.3 and 79.6 wt % carbon content, which is more as compared to simple carbons i.e. SC-C and SC-W having 70.1 and 64.6 wt %.

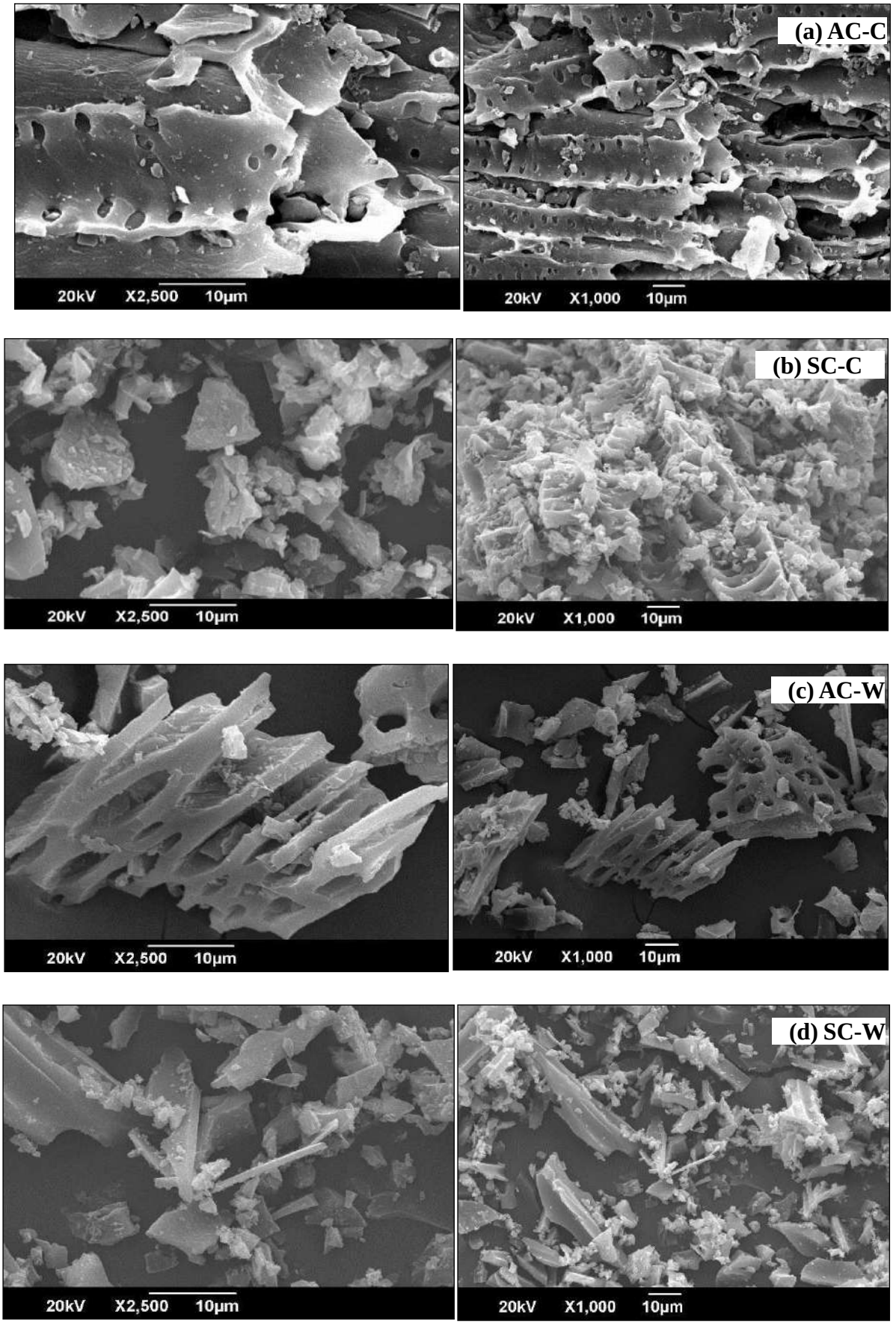

Figure 15. SEM images of maize cob and wood scraps (a) AC-C (b) SC-C (c) AC-W (d) SC-W

The EDX data indicates that all the prepared samples are composed of carbon, oxygen, and nitrogen (Figure 16). EDX data confirms that the AC-C and AC-W has higher proportion of carbon content i. e. 80.3 and 79.6 wt% compared to simple carbons i. e. SC-C and SC-W having 70.1 and 64.6 wt% (Table 1).

Table 4. Elemental composition of all prepared carbon materials

Elemental composition of AC-C

Element	**Weight %**	**Atomic %**
C	80.3	84.2
N	2.9	2.6
O	16.7	13.2

Elemental composition of SC-C

Element	**Weight %**	**Atomic %**
C	70.1	76.2
N	8.3	7.7
O	18.4	15.0

Elemental composition of AC-W

Element	**Weight %**	**Atomic %**
C	79.6	83.4
N	6.6	6.0
O	13.3	10.5

Elemental composition of SC-W

Element	**Weight %**	**Atomic %**
C	64.6	72.5
N	9.8	9.4
O	18.6	15.7

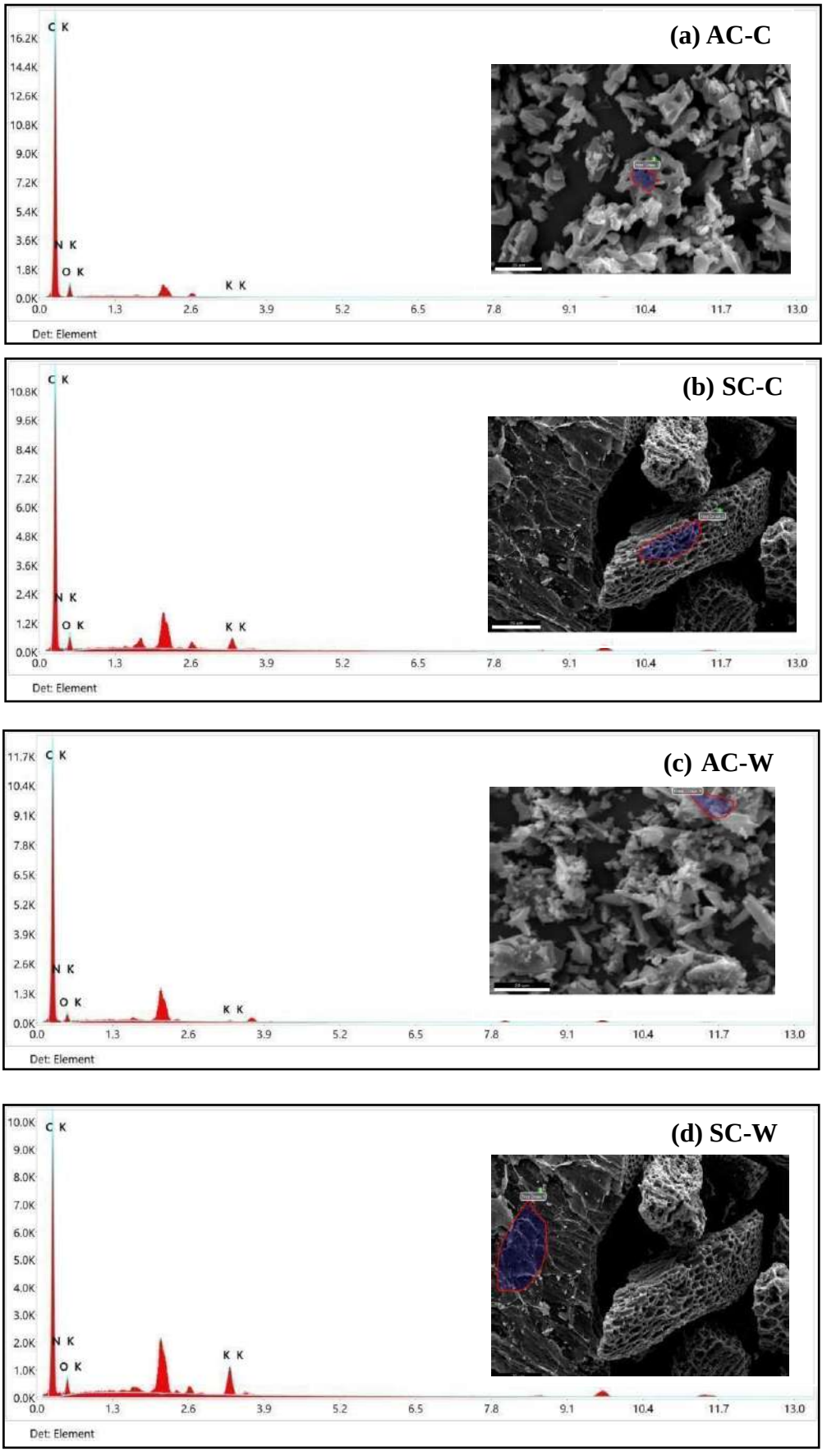

Figure 16. EDX micrographs of maize cob, and wood scraps (a) AC-C (b) SC-C (c) AC-W (d) SC-W

4.1.1.2 XRD

The phase structures of AC and SC samples of both biowastes were characterized by XRD. Figure 17 shows the XRD patterns of all the samples of study. Figure 17 exhibits two broad and low intensity carbonaceous peaks of maize cob samples around 28° and 47° as well as of wood scraps samples around 22° and 44° corresponding to the plane of graphite, demonstratingthe formation of amorphous carbon and were matched with standard JCPDS No. 75-1621 [103].The AC-C showed an additional peak at 15° (shown as *) indicates more oxygen functional groups in the sample. The diffraction peaks associated to the intercalated K^+ ions werecompletely disappeared when the carbonization temperature was raised such as in the case AC-C and AC-W samples. Both the activated carbon samples show a broad peak at 28° (AC-C), 22°(AC-W) and a weak peak at 47° (AC-C), 44° (AC-W) are attributed to the plane of the graphitic carbon as shown in figure 8b [104, 105]. It must be noted that the high level of graphitization is greatly beneficial to improve electrical conductivity and more defective (porous) sites for the improvement of electrolyte ions adsorption [106]. The observed diffraction lines are significantly broader that indicates the more amorphous and disordered nature of simple carbon samples [107].

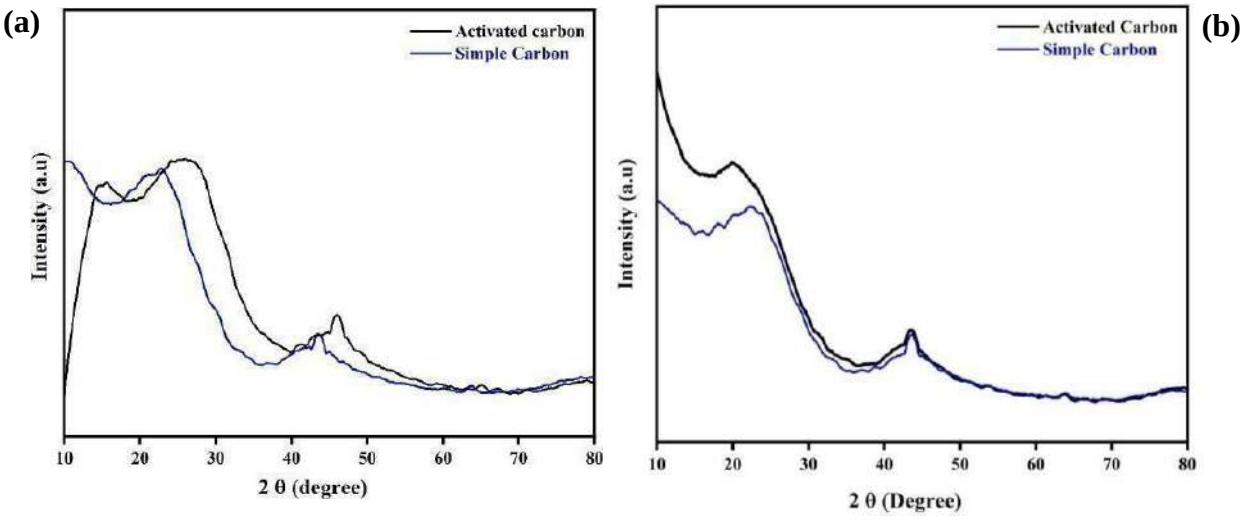

Figure 17. XRD peaks of maize cob and wood scraps (a) AC-C, SC-C (b) AC-W, SC-W

4.1.1.3 Fourier Transform Infrared Spectroscopy (FTIR)

FT-IR spectrum of all prepared samples (AC-C, SC-C, AC-W, SC-W) was conducted to study the chemical composition (functional groups) of samples at wavelength from 400 to 4000 cm^{-1}. The O-H stretching observed around 3395 cm^{-1} was mainly attributed to chemisorbed water

molecules and hydroxyl groups on the materials. And, the C-H the observed stretching around 2895 cm^{-1}. While the C=C stretching around 1625 cm^{-1} are assigned to the characteristic olefinic group it shows that the graphitization is very much increased for AC-C and AC-W. Compared to SC-C and SC-W, the number of vibrational modes is largely diminished due to the reduction of functional groups in the AC-C and AC-W [108].

Moreover, if compare the results of simple carbon and activated carbon, it is concluded that peaks of AC-C and AC-W are higher over SC-C and SC-W. The distance between simple and activated carbon is higher which indicates that AC-C and AC-W were successfully activated by KOH.

On the other hand, if compare peaks of both the biowastes, then it can be concluded that there is a huge difference/distance between SC-C and AC-C compared to SC-W and AC-W that means AC-C can be considered as the best sample in terms of holding high conductivity efficiency among others (Figure 18).

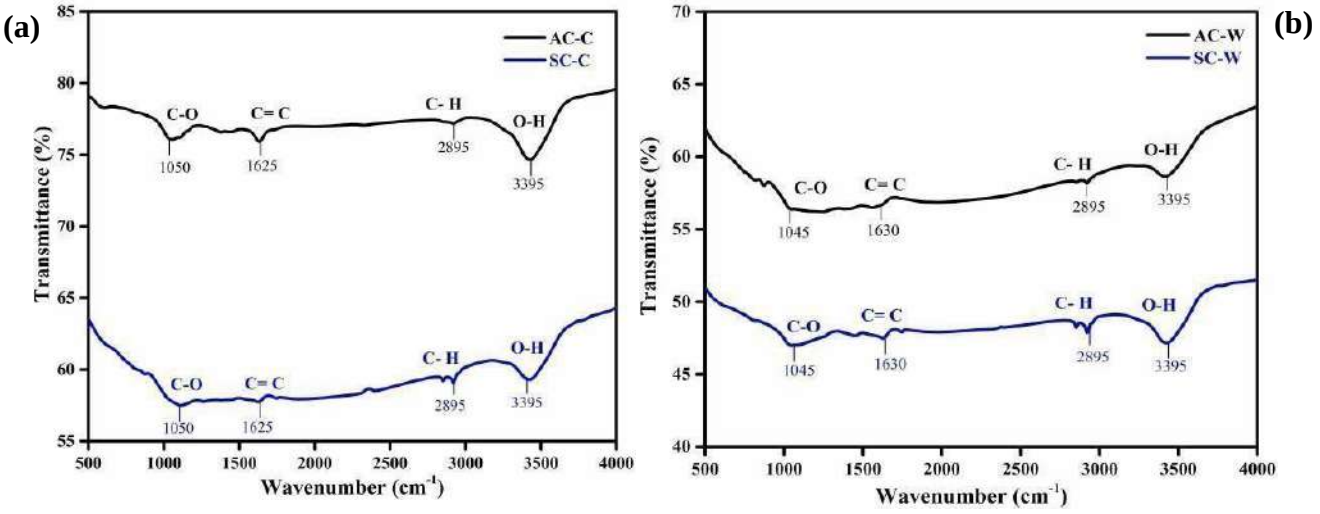

Figure 18. FTIR spectrum of maize cob, and wood scraps (a) AC-C, SC-C (b) AC-W, SC-W

4.1.1.3 Thermogravimetric analysis (TGA)

The TGA analysis of the prepared materials is displayed in Figure 19 (a, b). Considering the AC-C, almost or less than 20% weight was lost at 40 ˚C and makes sure KOH activated sample is more stable. While in case of SC-C, a major almost or less than 20 % or more weight loss was detected at 40 ˚C or below 100 ˚C which explains large amount of moisture lost which was adsorbed physically, then sample was stable temperature along a bit steady loss in weight up until 400 ˚C which represents maybe water synchronized within the pores of the materials, and then there was a major reduction in weight from 400 ˚C to 600 ˚C which can be explained by the disintegration of the sample. Similarly, with carbon materials of wood scraps SC-W, AC-W, the pattern of only AC-W represents an initial mass loss below 100 ˚C which attributes to the loss of adsorbed water. Likewise, samples of maize cob, the second major mass loss starts at 430 ˚C attributes to the disintegration of sample and loss of organic elements present in the samples of wood scraps [108]. The weight-loss trend in carbon materials shows a sharp decrease of weight after 430 ˚C, then there is a continuous gradual loss in weight until 580-750 ˚C which attributes to the gradual decomposition of sample.

Briefly, if compare the stability results of both biowastes (maize cob and wood waste). It is concluded that there is no significant difference in thermal stability of both biowastes. But can yet say, AC-C is more stable as having the TGA profile more in order when compared to other samples indicating that the KOH activation results the formation of structurally stable carbon atoms. Besides that, we can say that both biowaste carbon materials are stable till 430 ˚C while after this range of temperature, both biowastes samples lost their stability and decomposed as a result.

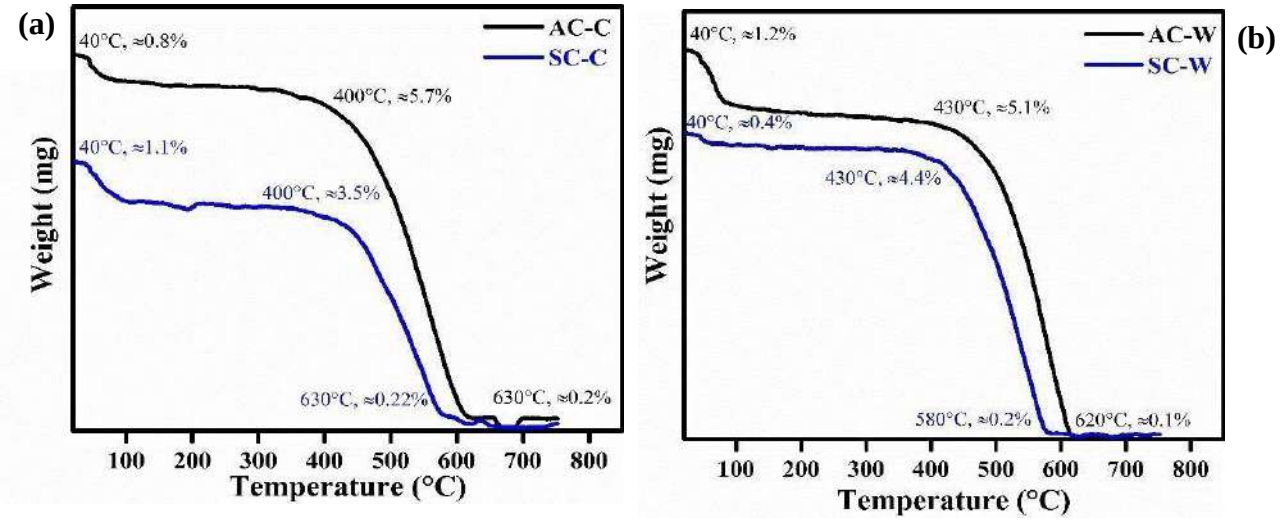

Figure 19. TGA curves of maize cob and wood scraps (a) AC-C, SC-C (b) AC-W, SC-W

4.1.1.4 Raman Spectroscopy

Raman spectroscopy is a potential analytical tool to evaluate the degree of functionalization before and after carbonization/activation in the bio-derived carbon materials (Figure 20). Usually, the intensity ratio (I_D/I_G) of D band (I_D) and G band (I_G) reveals the degree of defective nature and the extend of graphitization. The D peak is caused by out of plane vibrations related to the existence of structural defects. Whereas the G peak is caused by in-plane vibrations of sp^2 linked carbon atoms. The sp^3/sp^2 carbon ratio is related to the D/G ratio. The Raman spectrum of simple and activated carbons of maize cob is shown in Figure 20a. The two distinct peaks which correspond to the D and G bands at 1351.21 and 1572.23 cm^{-1} are shown for the activated carbon of maize cob. The peak intensity of these two bands (D/G) is calculated to be 0.85 as an index to suggest the crystallinity and to estimate the defects of carbon compounds. It indicates that the KOH-activation process increased the degree of graphitization by removal of surface functional group and defect structure, which is in good agreement with the FT-IR observations. While, 1330.23 and 1536.98 cm^{-1} peaks are shown for the simple carbon of cob, D/G is calculated to be 0.86. Likewise, in Figure 5b, two distinct peaks at 1330.21 and 1523.31 cm^{-1} were observed for the activated carbon of wood and the D/G was found to be 0.86 while at 1320.31 and 1513.21 cm^{-1} are for the simple carbon of wood (D/G = 0.87). It also indicates that in case of activated carbon of wood, KOH activation process increased the degree of graphitization by removal of surface functional group. The D/G value 0.86 also indicating a higher electronic conductivity. While in SC-C, D/G ratio 0.87 implicit that more lattice defects emerged and lesser conductivity behavior [109].

To summarize, if compare Raman results of both biowastes, the highest intensity (I_D/I_G) ratio of the wood waste material (SC-W, AC-W) suggests the AC-W has highest degree of the graphitization or highest disordered carbon skeleton in the matrices compared to other synthesized carbon material SC-W. So, it can be concluded that SC-W has lowest intensity I_D/I_G ratio indicates that lowest degree of graphitization means less presence of deformity in sample. It makes sure AC-C is the most efficient sample to be made as well as proved to have higher conductivity among rest of others.

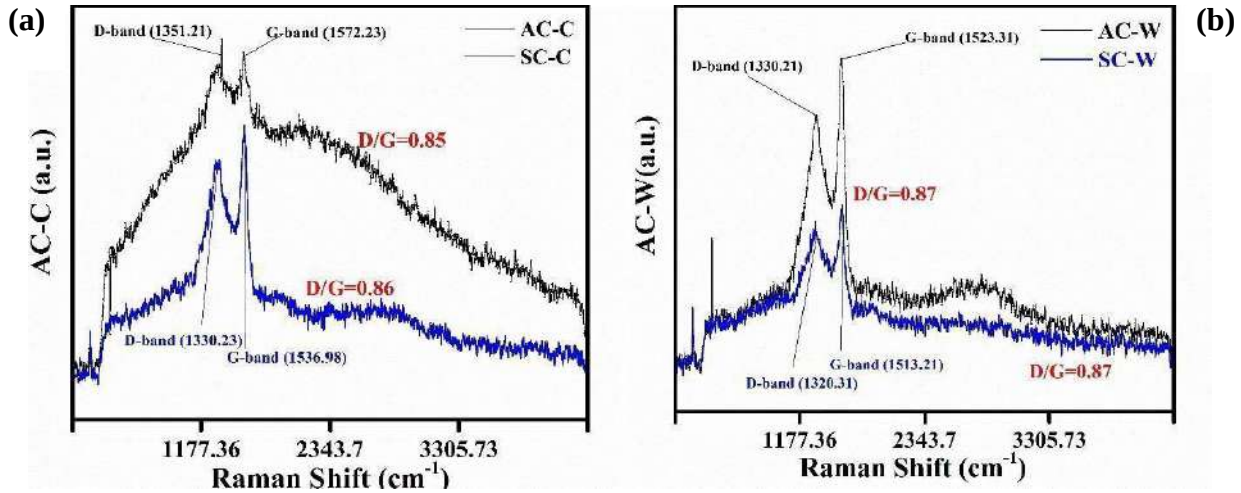

Figure 20. Raman spectrum of maize cob, and wood scraps (a) AC-C, SC-C & (b) AC-W, SC-W

4.2 Electrochemical capacitive performance of the prepared activated materials

4.2.1 Three electrode testing

The three-electrode testing was conducted to check the electrochemical properties of the samples, CV curves and GCD curves were performed with 6 M KOH aqueous electrolyte in a three-electrode system. Figure 21 (a, b) displays the CV curves of samples with a range of scan rates of 10, 15, 20, 30, 50, 80 and 100 $mV.s^{-1}$ at the voltage window from 0 to 0.6 V. Obviously, the CV curves of samples present a rectangular shape, indicating good electric-double layer capacitance (EDLCs) characteristics. The area bounded by the CV curve of AC-C is distinctly larger than the other (AC-W), demonstrating the best specific capacitance [110]. The enhanced capacitance of AC-C compared with other sample AC-W is attributed to the appropriate hierarchical pore structure and large SSA for easily electrolytes ionic transport and storage. The CV curves of both activated carbon samples remain rectangular shape even at high scan rate of 100 $mV.s^{-1}$, showing fast charge propagation kinetics with good reversibility. If compare the CV results of both activated carbon samples (AC-C & AC-W); AC-C in conclusion has better results compared to AC-W. Because in case of AC-C, the curves at 100 $mV.s^{-1}$ are higher than AC-W peaks at 100 $mV.s^{-1}$.

The GCD curves of both activated carbon samples were investigated from 0 to 0.6 V at different current densities 5, 8, 10, 20, 25 $A.g^{-1}$ shown in Figure 21 (c, d). The specific capacitance values of AC-C are 535.75, 307.34, 214.28, 75.76 and 54.875 $F.g^{-1}$, respectively, which are calculated from discharge curves. On the other hand, the specific capacitance values for AC-W are 135.64, 80.76, 70.36, 30.93 and 15 $F.g^{-1}$ which are lower in comparison to AC-C. In comparison of both the samples AC-C and AC-W, the AC-C reveals a largest specific capacitance, which is consistent with CV curves. The GCD curves show symmetric triangular shapes and nearly linear potential–time behavior, further suggesting an ideal capacitive feature and excellent reversibility [110].

In three-electrode system, when the current density increases from 5 to 25 $A\ g^{-1}$, AC-C shows 98.79% initial capacitance retention shown in Figure 9 (f), suggesting an excellent rate capability. After 10,000 cycles at 250 µA, the AC-C exhibits good cyclic stability with 99.81% retention of initial capacitance. It should be noted that the KOH activation shows a good repeatability. While AC-W shows 95.43% initial capacitance retention and after 10k cycles at 250 µA achieves 97.67% retention. So, in conclusion, the AC-C has excellent capacitance retention compared to AC-W.

4.2.2 Two electrode testing

4.2.2.1 Fabrication of symmetrical electrode system for device testing

A symmetrical SC was fabricated and measured in a 6 M KOH aqueous electrolyte in order to check the real practical applications of AC-C and AC-W electrodes. The wide working voltage window in the potential region of 0–0.6 V is a prerequisite for high energy density SCs. The CV of both samples (Figure 22 a, b) was done in an aqueous electrolyte KOH at diverse sweep rates (10 to 100 $mV.s^{-1}$) and showed quasi rectangular voltammogram. Likewise, the GCD (Figure 22 c, d) was done at diverse current densities exhibited a quasi-triangular curve which again prove the EDLC nature of the device [111]. Notably, the AC-C symmetric SCs keeps a good rectangular form even at 100 mV/s, indicating rapid charge transfer rate and excellent rate characteristic. Fig. displays the GCD curves of the AC-C and AC-W at different current densities display high symmetry at all current densities, indicating good kinetic reversibility [112, 113]. In comparison of both the samples AC-C and AC-W, the AC-C reveals a largest specific capacitance 347.71 $F.g^{-1}$ at 5 $A.g^{-1}$, which is consistent with CV curves.

The electrochemical performance of supercapacitors based on the KOH-activated materials was measured in a three-electrode (Fig 21e) as well as in two-electrode configuration (Fig 22e)in the presence of a 6 M KOH aqueous electrolyte solution. Figure shows the Nyquist plots of AC-C and AC-W as electrode materials in 6 M KOH, across a frequency range of 10 kHz to 100 kHz. In the low frequency zone, there is a nearly vertical straight line (C_{dl}) indicating good EDLC behavior [114, 115]. There's also a short 45° slope at the low frequency region describedto be the Warburg impedance (W). It is reported that W is related to the diffusion of ions into the pore channels of electrode materials [116, 117]. While at high frequency area, there are two features: (1) solution resistance (R_s), including the intrinsic resistance of electrode materials, ionic resistance of electrolyte and contact resistance between electrode and current collector; (2) charge transfer resistance (R_{ct}), showing as a small semicircle. The estimated values of R_s and R_{ct} of AC-C and AC-W in three-electrode are 4.75 Ω and 5.3 Ω while in two-electrode are 5.2 Ω and 6.1 Ω, respectively indicating good conductivity in aqueous electrolytes (Table 4). As the figure shows that the AC-C electrode has lower R_s and R_{ct} than the other electrodes, indicating that ion transfer at the electrode/electrolyte interface is improved. In the case of AC-C, the slope above 45◦ can be attributed to the behavior of the ideal capacitor [118].

Table 5. Resistance values of all prepared carbon materials

Electrodes (3E)	**R_s**	**R_{ct}**	**ESR**
AC-C	0.45	4.3	4.75
AC-W	0.8	4.5	5.3
Electrodes (2E)	**R_s**	**R_{ct}**	**ESR**
AC-C	1.0	4.2	5.2
AC-W	1.6	4.5	6.1

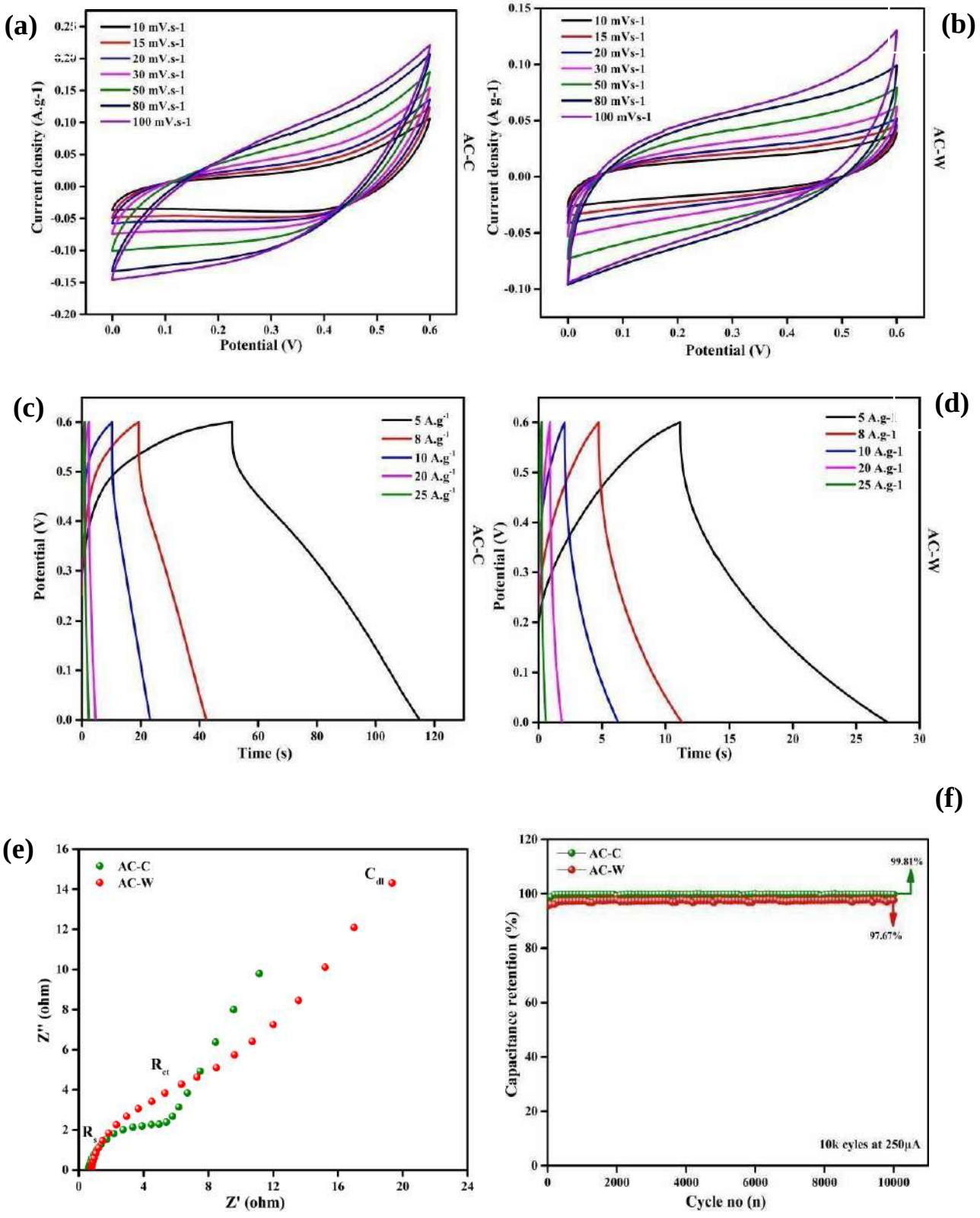

Figure 21: Electrochemical properties of prepared activated carbons in a three-electrode system (3E) with 6 M KOH electrolyte solution (a), (b) CV curves of AC-C & AC-W at 10, 15, 20, 30, 50, 80, 100 mV.s $^{-1}$ (c), (d) GCD curves of AC-C & AC-W at 5, 8, 10, 20, 25 A.g^{-1}. (e) Nyquist plots of AC-C & AC-W (f) Cyclic stability of AC-C & AC-W at 250 µA

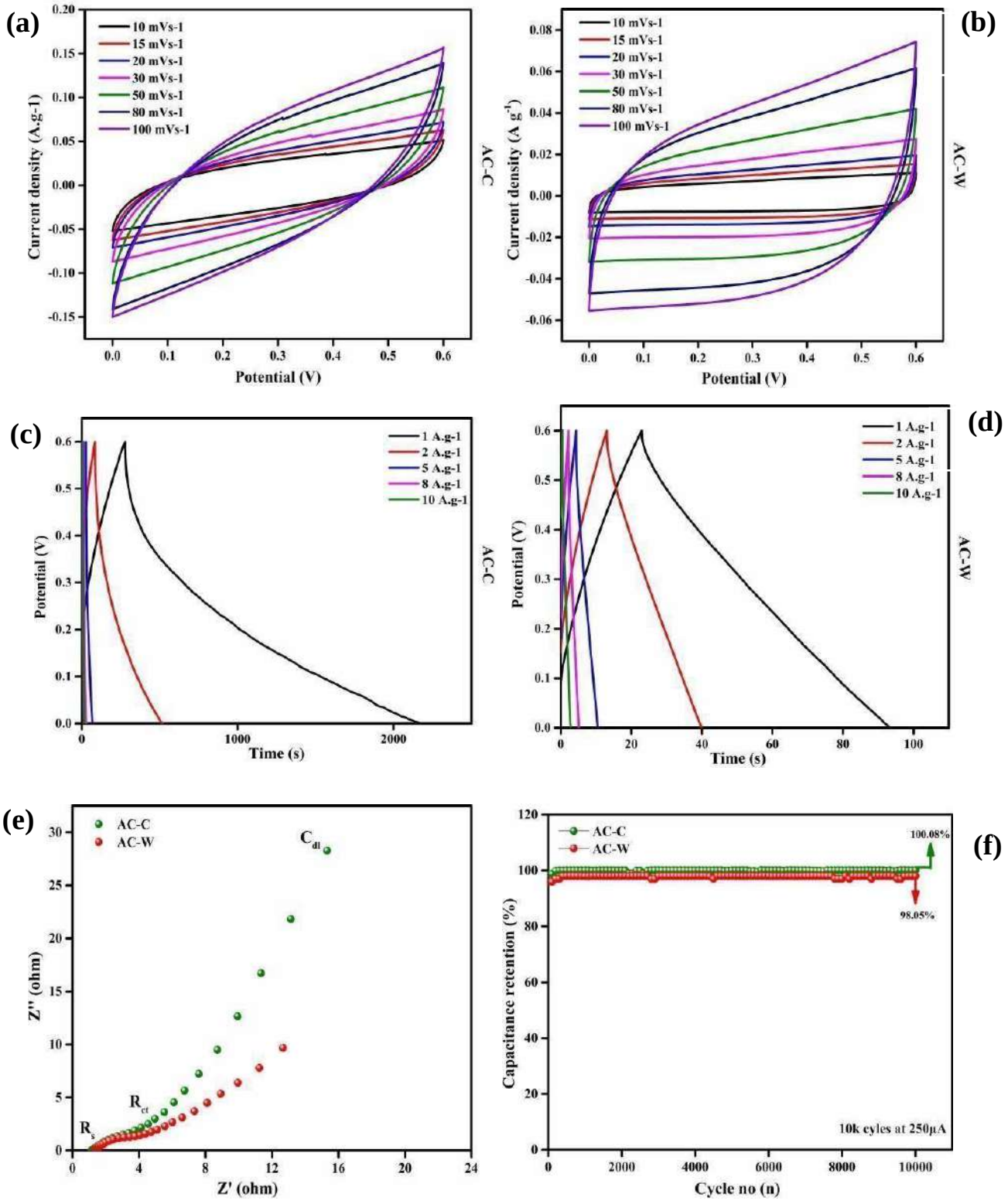

Figure 21. Electrochemical properties of prepared activated carbons in a two-electrode (2E) symmetric system with 6 M KOH electrolyte solution (a), (b) CV curves of AC-C & AC-W at 10, 15, 20, 30, 50, 80, 100 mV.s $^{-1}$ (c), (d) GCD curves of AC-C & AC-W at 1, 2, 5, 8 and 10 A.g^{-1}. (e) Nyquist plot of AC-C & AC-W (f) Cyclic stability of AC-C & AC-W at 250 µA

Conclusion

The as-obtained ACs from maize cob and wood scraps were made in the current work using a straightforward process and employed as electrode materials for EDLCs. The performance of the electrode materials was shown to be highly influenced by the synthesis parameters of activation temperature at 700 °C. When activated carbon from wood and maize cob was electrochemically analyzed, an EDLC charge storage mechanism was shown, with specific capacitances of 535.75 and 135.64 $F.g^{-1}$ at 5 $A.g^{-1}$, respectively. Additionally, AC-C has great cyclic stability and rate capability, with 99.81% of the capacitance remaining after 10,000 cycles at 250 µA. In comparison to wood waste, corncob performed better. It can be due to larger aromatic rings of C=C, less moisture content and rougher morphology with smaller particle size. This study reveals efficient method to reuse waste materials but further studies related to optimization, underlying mechanism, and porosity control on activated carbon can lead to enhanced performance of the EDLC supercapacitor.

References

1. Sneddon, G., Greenaway. A., & Yiu, H.H.P. (2014). The Potential Applications of Nanoporous Materials for the Adsorption, Separation, and Catalytic Conversion of Carbon Dioxide. Advanced Energy Materials, 4 (10), 1301873.

2. Sun, M.H., Huang, S.Z., Chen, L.H., Li, Y., Yang, X.Y., Yuan, Z.Y., & Su, B.L. (2016) Applications of hierarchically structured porous materials from energy storage and conversion, catalysis, photocatalysis, adsorption, separation, and sensing to biomedicine. Chemical Society Review, 45, 3479. doi: : 10.1039/c6cs00135a

3. Sakintuna, B., & Yurum, Y. (2005). Templated Porous Carbons: A review article. Industrial Engineering Chemistry Research, 44(9), 2893-2902. doi: 10.1021/ie049080w

4. Titirici, M.-M., White, R. J., Falco, C., & Sevilla, M. (2012). Black perspectives for a green future: Hydrothermal carbons for environment protection and energy storage. Energy & Environmental Science, 5, 6796-6822.

5. Xin, W., & Song, Y. (2015) Mesoporous carbons: Recent advances in synthesis and typical applications. Royal Society of Chemistry Advances, 5, 83239-83285.

6. Wang, J., Nie, R., Ding, B., Dong, S., Hao, X., Dou, H., & Zhang, X. (2017) Biomass derived carbon for energy storage devices. Journal of Materials Chemistry A, 5, 2411-2428.

7. Yao, Y., Zhang, Q., lui, P., Yu, P., Huang, L., Zeng, S.Z., Lui, L., Zheng, X., & Zou, J. (2018). Facile synthesis of high-surface-area nanoporous carbon from biomass resources and its application in supercapacitors. Royal Society of Chemistry Advances, 8, 1857-1865.

8. BP p.l.c., (2017), BP's Energy Outlook 2017 edition.

9. World Energy Council, World Energy Scenarios: Composing energy futures to 2050. (2013: England)

10. Eurostat, Renewable statistics. (2018).

11. EREC, Renewable Energy Target by Europe by 2020. 2013, European Renewable Energy Council.

12. Conway, B.E., Electrochemical Supercapacitors: Scientific Fundamentals and Technological Applications. 1999: Springer US.

13. Gonzalez, F., Electrochemical Double Layer Capacitors: Supercapacitors 2014-2024.

14. Yu, G., et al., (2013), Hybrid nanostructured materials for high-performance electrochemical capacitors. Nano Energy, 2(2): p. 213-234.

15. Holmberg, S., et al., (2014), 3-D Micro and Nano Technologies for Improvements in Electrochemical Power Devices. Micromachines, 5(2): p. 171.

16. Wang, X., et al., (2017) Enhancing capacitance of supercapacitor with both organic electrolyte and ionic liquid electrolyte on a biomass-derived carbon. RSC Advances, 7(38): p. 23859- 23865.

17. Yu, A., V. Chabot, and J. Zhang, (2017), Electrochemical Supercapacitors for Energy Storage and Delivery: Fundamentals and Applications: CRC Press.

18. Zhang, L.L. and X.S. Zhao, (2009), Carbon-based materials as supercapacitor electrodes. Chemical Society Reviews, 38(9): p. 2520-2531.

19. Dubal, D.P., et al., (2015), Hybrid energy storage: the merging of battery and supercapacitor chemistries. Chemical Society Reviews, 44(7): p. 1777-1790.

20. Abioye, A.M. and F.N. Ani, (2015) Recent development in the production of activated carbon electrodes from agricultural waste biomass for supercapacitors: A review. Renewable and Sustainable Energy Reviews, 52: p. 1282-1293.

21. Jin, Y., et al., (2016), Hierarchical porous microspheres of activated carbon with a high surface area from spores for electrochemical double-layer capacitors. Journal of Materials Chemistry A, 4(41): p. 15968-15979.

22. Zhang, T., et al., (2004), Preparation of activated carbon from forest and agricultural residues through CO_2 activation. Chemical Engineering Journal, 105(1–2): p. 53-59.

23. Weinstein, L. and R. Dash, (2013), Supercapacitor carbons. Materials Today, 16(10): p. 356-357.

24. Burke, A., (2007), R&D considerations for the performance and application of electrochemical capacitors. Electrochimica Acta, 53(3): p. 1083-1091.

25. Jäckel, N., et al., (2014), Comparison of carbon onions and carbon blacks as conductive additives for carbon supercapacitors in organic electrolytes. Journal of Power Sources, 272: p. 1122- 1133.

26. Beguin, F. and E. Frackowiak, (2009), Carbons for Electrochemical Energy Storage and Conversion Systems. 2009: CRC Press.

27. Stoller, M.D. and R.S. Ruoff, (2010), Best practice methods for determining an electrode material's performance for ultracapacitors. Energy & Environmental Science, 2010. 3(9): p. 1294-1301.

28. Jong H., K., et al., (2001) The effect of Nickel Foam current collector in carbo electrode based electric double layer capacitor. Electrochemistry - Tokyo, 69(11): p. 5.

29. Gu, W. and G. Yushin, (2014), Review of nanostructured carbon materials for electrochemical capacitor applications: advantages and limitations of activated carbon, carbide-derived carbon,zeolite-templated carbon, carbon aerogels, carbon nanotubes, onion-like carbon, and graphene.Wiley Interdisciplinary Reviews: Energy and Environment, 3(5): p. 424-473.

30. Saito, M., et al., (2017), Strategies for fast ion transport in electrochemical capacitor electrolytes from diffusion coefficients, ionic conductivity, viscosity, density and interaction energies based on HSAB theory. RSC Advances, 7(24): p. 14528-14535.

31. Jäckel, N., et al., (2016), Increase in Capacitance by Sub nanometer Pores in Carbon. ACS Energy Letters, 1(6): p. 1262-1265.

32. Kashkooli, A.G., et al., (2015), Effects of structural design on the performance of electrical double layer capacitors. Applied Energy, 138: p. 631-639.

33. Zhang, Y., et al., (2009), Progress of electrochemical capacitor electrode materials: A review. International Journal of Hydrogen Energy, 34(11): p. 4889-4899.

34. Smith, T.J. and K.J. Stevenson, (2007) - Reference Electrodes A2 - Zoski, Cynthia G, in Handbook of Electrochemistry. Elsevier: Amsterdam. p. 73-110.

35. Zhang, S. and N. Pan, (2015) Supercapacitors performance evaluation. Advanced Energy Materials, 5(6)

36. Rennie, A., et al., (2011), Nitrogen-enriched Carbon Materials for High-power Electrochemical Capacitors: University of Strathclyde.

37. Zhong, C., et al., (2015), A review of electrolyte materials and compositions for electrochemical supercapacitors. Chemical Society Reviews, 44(21): p. 7484-7539.

38. Zeller, M., et al., (2012), Relationship Between Structural Properties and Electrochemical Characteristics of Monolithic Carbon Xerogel-Based Electrochemical Double-Layer Electrodes in Aqueous and Organic Electrolytes. Advanced Energy Materials, 2(5): p. 598-605.

39. Zhou, S.-Y., et al., (2007), Effect of activated carbon and electrolyte on properties of supercapacitor. Transactions of Nonferrous Metals Society of China, 17(6): p. 1328- 1333.

40. Bello, A., et al., (2016), Renewable pine cone biomass derived carbon materials for supercapacitor application. RSC Advances, 6(3): p. 1800-1809.

41. Peng, C., et al., (2013), Promising activated carbons derived from waste tea-leaves and their application in high performance supercapacitors electrodes. Electrochimica Acta, 87: p. 401-408.

42. Qian, W., et al., (2014) Human hair-derived carbon flakes for electrochemical supercapacitors. Energy & Environmental Science, 7(1): p. 379-386.

43. Wang, K., et al., (2015), Promising biomass-based activated carbons derived from willow catkins for high performance supercapacitors. Electrochimica Acta, 166: p. 1-11.

44. Wang, X., et al., (2016), Low-cost, green synthesis of highly porous carbons derived from lotus root shell as superior performance electrode materials in supercapacitor. Journal of Energy Chemistry, 25(1): p. 26-34.

45. Zhan, C., et al., (2016), Flour food waste derived activated carbon for high-performance supercapacitors. RSC Advances, 6(92): p. 89391-89396.

46. Ferrero, G.A., A.B. Fuertes, and M. Sevilla, (2015), From Soybean residue to advanced supercapacitors. Scientific Reports, 5: p. 16618.

47. Ruan, C., K. Ai, and L. Lu, (2014), Biomass-derived carbon materials for high-performance supercapacitor electrodes. RSC Advances, 4(58): p. 30887-30895.

48. Sudhan, N., et al., (2017), Biomass-Derived Activated Porous Carbon from Rice Straw for a High Energy Symmetric Supercapacitor in Aqueous and Non-aqueous Electrolytes. Energy &Fuels, 31(1): p. 977-985.

49. Adinaveen, T., et al., (2015), Surface and porous characterization of activated carbon prepared from pyrolysis of biomass (rice straw) by two-stage procedure and its applications in supercapacitor electrodes. Journal of Material Cycles and Waste Management, 17(4): p. 736-747.

50. Pandolfo, A.G. and A.F. Hollenkamp, (2006) Carbon properties and their role in supercapacitors. Journal of Power Sources, 157(1): p. 11-27.

51. Kötz, R. and M. Carlen, (2000), Principles and applications of electrochemical capacitors.

Electrochimica Acta, 45(15): p. 2483-2498.

52. Wessells, C., et al., (2010) Investigations of the Electrochemical Stability of Aqueous Electrolytes for Lithium Battery Applications. Electrochemical and Solid-State Letters, 13(5): p. A59- A61.

53. Dai, Z., et al., (2015), Cell voltage versus electrode potential range in aqueous supercapacitors. Scientific Reports, 5: p. 9854.

54.Tomiyasu, H., et al., (2017), An aqueous electrolyte of the widest potential window and its superior capability for capacitors. Scientific Reports, 7: p. 45048.

55. Zhong, C., et al., (2016), Electrolytes for Electrochemical Supercapacitors: CRC Press.

56. Dincer, I., (2016), Comprehensive Energy Systems. 2018: Elsevier Science.

57. Kim, M., I. Oh, and J. Kim, (2015), Effects of different electrolytes on the electrochemical and dynamic behavior of electric double layer capacitors based on a porous silicon carbide electrode. Physical Chemistry Chemical Physics, 17(25): p. 16367-16374.

58. Armand, M., et al., (2009), Ionic-liquid materials for the electrochemical challenges of the future. Nature Materials, 8: p. 621.

59. Wasserscheid, P. and T. Welton, (2003), Ionic Liquids in Synthesis. Organic Process Research & Development, 7(2): p. 223-224.

60. Kumar, V. and S.V. Malhotra, (2010), Ionic Liquids as Pharmaceutical Salts: A Historical Perspective, in Ionic Liquid Applications: Pharmaceuticals, Therapeutics, and Biotechnology American Chemical Society. p. 1-12.

61. Rodriguez Castillo, A.S., et al., (2017), Physicochemical properties of some hydrophobic room temperature ionic liquids applied to volatile organic compounds biodegradation processes. Journal of Chemical Technology & Biotechnology, 93(1): p. 215-223.

62. N oofeli, A., P.J. Hall, and A.J.R. Rennie, (2014), Ionic liquid based EDLCs: influence of carbon porosity on electrochemical performance. Faraday Discussions, 172(0): p. 163-177.

63. Martins, V.L., et al., (2017), Improved Performance of Ionic Liquid Supercapacitors by using Tetra-cyanoborate Anions. Chem Electro.

64. Pohlmann, S., et al., (2013), The influence of pore size and surface area of activated carbons on the performance of ionic liquid based supercapacitors. Physical Chemistry Chemical

Physics, 15(40): p. 17287-17294.

65. Gu, W. and G. Yushin, (2014), Review of nanostructured carbon materials for electrochemical capacitor applications: advantages and limitations of activated carbon, carbide-derived carbon, zeolite-templated carbon, carbon aerogels, carbon nanotubes, onion-like carbon, and graphene. Wiley Interdisciplinary Reviews: Energy and Environment, 3(5): p. 424- 473.

66. Hall, P.J., et al., (2010), Energy storage in electrochemical capacitors: designing functional materials to improve performance. Energy & Environmental Science, 3(9): p. 1238-1251

67. Koh, A.R., et al., (2014), The effect of the ionic size of small quaternary ammonium BF4 salts on electrochemical double layer capacitors. Physical Chemistry Chemical Physics, 16(29):p. 15146-15151.

68. Huang, M.-M., et al., (2011), Static relative dielectric permittivities of ionic liquids at 25 C. Journal of Chemical & Engineering Data, 56(4): p. 1494-1499.

69. Kim, D., P.K. Kannan, and C.-H. Chung, (2018), High-Performance Flexible Supercapacitors Based on Ionogel Electrolyte with an Enhanced Ionic Conductivity. Chemistry Select, 3(7): p. 2190-2195.

70. Wang, G., L. Zhang, and J. Zhang, (2012), A review of electrode materials for electrochemical supercapacitors. Chem Soc Rev, 41(2): p. 797-828.

71. Lozano-Castelló, D., et al., (2003), Influence of pore structure and surface chemistry on electric double layer capacitance in non-aqueous electrolyte. Carbon, 2003. 41(9): p. 1765-1775.

72. He, Y., (2017), Capacitive Mechanism of Oxygen Functional Groups on Carbon Surface in Supercapacitors. arXiv preprint arXiv:1704.08405.

73. Kikuchi, K., et al., (2013), Double Layer Properties of Spent Coffee Grounds-derived Carbon Activated with Potassium Hydroxide (KOH). Electrochemistry, 81(10): p. 828-832.

74. Shi, H., (1996), Activated carbons and double layer capacitance. Electrochimica Acta, 41(10): p. 1633-1639. 163

75. Wang, J. and S. Kaskel, (2012), KOH activation of carbon-based materials for energy storage. Journal of Materials Chemistry, 22(45): p. 23710-23725.

76. Yang, H., et al., (2013), Achieving Both High Power and Energy Density in

Electrochemical Supercapacitors with Nanoporous Graphene Materials. arXiv preprint arXiv:1311.1413.

77. Zhang, L.L., R. Zhou, and X.S. Zhao, (2010), Graphene-based materials as supercapacitor electrodes. Journal of Materials Chemistry, 20(29): p. 5983.

78. Quintero, R., et al., (2014), Carbon nanotube 3D current collectors for lightweight, high performance and low-cost supercapacitor electrodes. RSC Advances, 4(16): p. 8230- 8237.

79. Kurig, H., et al., (2010), Electrochemical Characteristics of Titanium Carbide Derived Carbon|1- Ethyl-3-Methylimidazolium Tetrafluoroborate Electrical Double Layer Capacitors. ECS Transactions, 25(23): p. 15-23.

80. Song, W.-L., X. Li, and L.-Z. Fan, (2016), Biomass derivative/graphene aerogels for binder-free supercapacitors. Energy Storage Materials, 3: p. 113-122

81. Bryan, A.M., et al., (2016), Conducting polymers for pseudocapacitive energy storage. Chemistry of Materials, 28(17): p. 5989-5998.

82. Augustyn, V., P. Simon, and B. Dunn, (2014), Pseudocapacitive oxide materials for high-rate electrochemical energy storage. Energy & Environmental Science, 7(5): p. 1597-1614.

83. Lee, G., C.V. Varanasi, and J. Liu, (2015), Effects of morphology and chemical doping on electrochemical properties of metal hydroxides in pseudo-capacitors. Nanoscale, 7(7): p.3181-3188.

84. Liu, M., et al., (2014), Nitrogen-doped graphene nanoribbons as efficient metal-free electrocatalysts for oxygen reduction. ACS Appl Mater Interfaces, 6(6): p. 4214-22.

85. Ioannidou, O. and A. Zabaniotou, (2007), Agricultural residues as precursors for activated carbon production—A review. Renewable and Sustainable Energy Reviews, 11(9): p. 1966-2005.

86. Low, L.W., et al., (2015), Carbonization of Elaeis guineensis frond fiber: Effect ofheating rate and nitrogen gas flow rate for adsorbent properties enhancement. Journal of Industrial and Engineering Chemistry, 28: p. 37-44.

87. Li, A., et al., (2016), Effects of Temperature and Heating Rate on the Characteristics of Molded Biochar. Vol. 11.

88. Fu, P., et al., (2012), Evaluation of the porous structure development of chars from pyrolysis of rice straw: Effects of pyrolysis temperature and heating rate. Journal of Analytical and Applied Pyrolysis, 98: p. 177-183.

89. Cetin, E., R. Gupta, and B. Moghtaderi, (2005), Effect of pyrolysis pressure and heating rate on radiata pine char structure and apparent gasification reactivity. Fuel, 84(10): p. 1328-1334.

90. Ioannidou, O. and A. Zabaniotou, (2007), Agricultural residues as precursors for activated carbon production—A review. Renewable and Sustainable Energy Reviews, 11(9): p. 1966-2005.

91. Kim, D.-W., et al., (2017), Structural elucidation of physical and chemical activation mechanisms based on the microdomain structure model. Carbon, 114: p. 98-105.

92. Zhou, W., et al., (2016), Carbon Materials for Supercapacitors, in Nanomaterials in Advanced Batteries and Supercapacitors, K.I. Ozoemena and S. Chen, Editors. Springer International Publishing: Cham. p. 271-315.

93. Wang, J., et al., (2017), Biomass derived carbon for energy storage devices. Journal of Materials Chemistry A.

94. Deng, J., M. Li, and Y. Wang, (2016), Biomass-derived carbon: synthesis and applications in energy storage and conversion. Green Chemistry, 18(18): p. 4824-4854.

95. Genovese, M.; Jiang, J.H.; Lian, K.; Holm, N, (2015), High capacitive performance of exfoliated biochar nanosheets from biomass waste corn cob. J. Mater. Chem. A, 3, 2903–2913. [CrossRef]

96. J.S. Zhou, L. Hou, S.R. Luan, J.L. Zhu, H.Y. Gou, D. Wang, F.M. Gao, (2018), Nitrogen Co-doped Unique Carbon with 0.4 nm Ultra-Micropores for Ultrahigh Areal Capacitance Supercapacitors, Small 14, 1801897.

97. Y.B. Li, D.Y. Zhang, Y.M. Zhang, J.J. He, Y.L. Wang, K.J. Wang, Y.T. Xu, H.X. Li, Y. Wang, (2020), Biomass-derived microporous carbon with large micropore size for high performance supercapacitors, J. Power Sources 448, 227396.

98. S. Dutta, A. Bhaumik, K.W. Wu, (2014), Hierarchically porous carbon derived from polymers and biomass: Effect of interconnected pores on energy applications, Energy Environ.Sci 7;3574–3592.

99. C. Young, J.J. Lin, J. Wang, B. Ding, X.G. Zhang, S.M. Alshehri, T. Ahamad, R. R. Salunkhe, S.A. Hossain, J.H. Khan, Y. Ide, J. Kim, J. Henzie, K.C.-W Wu, N. Kobayashi, Y. Yamauchi, (2018), Significant Effect of Pore Sizes on Energy Storage in Nanoporous Carbon Supercapacitors, Chemistry - A European Journal 24;6127–6132.

100. Z. Andikaey, A.A. Ensafi, B. Rezaei, (2021), Iron-doped cobalt copper phosphide/ phosphate composite with 3D hierarchical flower-like structures as electrodes for hybrid supercapacitors, Electrochim. Acta 393, 139061, https://doi.org/ 10.1016/j.electacta.2021.139061.

101. Zhang, Q., Han, K.H., Li, S.J., Li, M., Li, J.X., Ren, K., (2018). Synthesis of garlic skin-derived 3D hierarchical porous carbon for high-performance supercapacitors. Nanoscale 10, 2427– 2437.

102. Ouyang, J., Wang, X., Wang, L., Xiong, W., Li, M., Hua, Z., Zhao, L., Zhou, C., Liu, X., Chen, H. and Luo, Y., (2022). Construction of a porous carbon skeleton in wood tracheids to enhance charge storage for high-performance supercapacitors.

103. Selvaraj, A., Chinnadurai, D., Cho, I., Bak, J. and Prabakar, K., (2022). Bio-waste wood-derived porous activated carbon with tuned microporosity for high performance supercapacitors. (XRD)

104. A.R. Selvaraj, I.S. Raja, D. Chinnadurai, R. Rajendiran, I. Cho, D.W. Han, K. Prabakar, (2022). Electrospun one dimensional (1D) pseudocapacitive nanorods embedded carbon nanofiber as positrode and graphene wrapped carbon nanofiber as negatrode for enhanced electrochemical energy storage, J. Energy Storage 46; 1–11, https://doi.org/10.1016/j.est.2021.103731.

105. A.R. Selvaraj, A. Muthusamy, H.-J. Inho-Cho, K. Kim, K. Prabakar Senthil, (2021), Ultrahigh surface area biomass derived 3D hierarchical porous carbon nanosheet electrodes for high energy density supercapacitors, Carbon N. Y. 174; 463–474, https://doi.org/10.1016/j.carbon.2020.12.052.

106. J. Wei, Y. Li, D. Dai, F. Zhang, H. Zou, X. Yang, Y. Ji, B. Li, X. Wei, (2020), Surface roughness: a crucial factor to robust electric double layer capacitors, ACS Appl. Mater. Interfaces 12:5786–5792, https://doi.org/10.1021/ acsami.9b18799.

107. B. Pal, S. Yang, S. Ramesh, V. Thangadurai, R. Jose, (2019), Electrolyte selection for supercapacitive devices: a critical review, Nanoscale Adv. 1, 3807–3835,

https://doi.org/10.1039/c9na00374f.

108. Karnan, M., Subramani, K., Srividhya, P. and Sathish, M., (2022). Electrochemical Studies on Corncob Derived Activated Porous Carbon for Supercapacitors Application in Aqueous and Non-aqueous Electrolytes.

109. Xu, M., Huang, Q., Lu, J. and Niu, J., (2022), Green synthesis of high-performance supercapacitor electrode materials from agricultural corncob waste by mild potassium hydroxide soaking and a one-step carbonization.

110. Ai, J., Yang, S., Sun, Y., Liu, M., Zhang, L., Zhao, D., Wang, J., Yang, C., Wang, X. and Cao, B., (2022), Corncob cellulose-derived hierarchical porous carbon for high performance supercapacitors.

111. A.R. Selvaraj, A. Muthusamy, H.-J. Inho-Cho, K. Kim, K. Prabakar Senthil, (2021), Ultrahigh surface area biomass derived 3D hierarchical porous carbon nanosheet electrodes for high energy density supercapacitors, Carbon N. Y. 174, 463–474, https://doi.org/10.1016/j.carbon.2020.12.052.

112. X. Liu, C. Lai, Z. Xiao, S. Zou, K. Liu, Y. Yin, T. Liang, Z. Wu, (2019), Superb electrolyte Penetration/Absorption of three-dimensional porous carbon nanosheets for multifunctional supercapacitor, ACS Appl. Energy Mater. 2, 3185–3193, https://doi.org/10.1021/acsaem.9b00002.

113. Y. Lin, Z. Chen, C. Yu, W. Zhong, (2019), Heteroatom-doped sheet-like and hierarchical porous carbon based on natural biomass small molecule peach gum for high performance supercapacitors, ACS Sustain. Chem. Eng. 7; 3389–3403, https://doi.org/10.1021/acssuschemeng.8b05593.

114. Z. Andikaey, A.A. Ensafi, B. Rezaei, (2021), Iron-doped cobalt copper phosphide/ phosphate composite with 3D hierarchical flower-like structures as electrodes for hybrid supercapacitors, Electrochim. Acta 393, 139061, https://doi.org/ 10.1016/j.electacta.2021.139061.

115. Z. Andikaey, A.A. Ensafi, B. Rezaei, (2020), Synthesis of engineered graphene nanocomposites coated with NiCo metal-organic frameworks as electrodes for high-quality supercapacitor, Int.J. Hydrog. Energy, https://doi.org/ 10.1016/j.ijhydene.2020.09.004.

116. J. Yan, C.E. Ren, K. Maleski, C.B. Hatter, B. Anasori, P. Urbankowski, A. Sarycheva, Y. Gogotsi, (2017), Flexible MXene/graphene films for ultrafast supercapacitors with outstanding

volumetric capacitance, Adv. Funct. Mater 27, 1701264.

117. Wu, M., Xu, S., Li, X., Zhang, T., Lv, Z., Li, Z. and Li, X., (2022), Pore regulation of woodderived hierarchical porous carbon for improving electrochemical performance.

118. M.F. Chen, D. Yu, X.Z. Zheng, X.P. Dong, (2019), Biomass based N-doped hierarchicalporous carbon nanosheets for all-solid-state supercapacitors, J. Energy Storage 21, 105–112.

Rabia Fatima_MS Research Thesis

ORIGINALITY REPORT

14%	8%	7%	3%
SIMILARITY INDEX	INTERNET SOURCES	PUBLICATIONS	STUDENT PAPERS

PRIMARY SOURCES

1	etheses.whiterose.ac.uk Internet Source	7%
2	Usman Ali Khan, Naseem Iqbal, Tayyaba Noor, Rabia Ahmad, Awais Ahmad, Junkuo Gao, Zain Amjad, Abdul Wahab. "Cerium based metal organic framework derived composite with reduced graphene oxide as efficient supercapacitor electrode", Journal of Energy Storage, 2021 Publication	2%
3	Rita Kumari, Surender Kumar Sharma, Vinamrita Singh, Chhaya Ravi Kant. "Facile, two-step synthesis of activated carbon soot from used soybean oil and waste engine oil for supercapacitor electrodes", Materials Today: Proceedings, 2022 Publication	1%
4	Mohammed Jalalah, Siddheswar Rudra, Belqasem Aljafari, Muhammad Irfan et al. "Sustainable synthesis of heteroatom-doped porous carbon skeleton from Acacia	1%

auriculiformis bark for high-performance symmetric supercapacitor device", Electrochimica Acta, 2022
Publication

5	Submitted to University of Wollongong Student Paper	1 %
6	M. Karnan, K. Subramani, P.K. Srividhya, M. Sathish. "Electrochemical Studies on Corncob Derived Activated Porous Carbon for Supercapacitors Application in Aqueous and Non-aqueous Electrolytes", Electrochimica Acta, 2017 Publication	<1 %
7	Xiao-Wei Chen, Olaf Timpe, Sharifah B.A. Hamid, Robert Schlögl, Dang Sheng Su. "Direct synthesis of carbon nanofibers on modified biomass-derived activated carbon", Carbon, 2009 Publication	<1 %
8	www.ncbi.nlm.nih.gov Internet Source	<1 %
9	worldwidescience.org Internet Source	<1 %
10	www.scribd.com Internet Source	<1 %
11	Swapnil Dharaskar, Pravin Kodgire, Praful Bansod. "Enhanced diesel properties with	<1 %

energy efficient nano-aluminium oxide and nano-cobalt oxide particles", Materials Today: Proceedings, 2021
Publication

---

12 Chun Wu, Junjie Cai, Qiaobao Zhang, Xiang Zhou, Ying Zhu, Pei Kang Shen, Kaili Zhang. "Hierarchical Mesoporous Zinc–Nickel–Cobalt Ternary Oxide Nanowire Arrays on Nickel Foam as High-Performance Electrodes for Supercapacitors", ACS Applied Materials & Interfaces, 2015 — <1%
Publication

---

13 Submitted to Middle East Technical University — <1%
Student Paper

---

14 Submitted to University of New England — <1%
Student Paper

---

15 magazine.uow.edu.au — <1%
Internet Source

---

16 Changjun Zhang, Haihui Zhou, Xiaoqing Yu, Dan Shan, Tingting Ye, Zhongyuan Huang, Yafei Kuang. "Synthesis of RuO2 decorated quasi graphene nanosheets and their application in supercapacitors", RSC Advances, 2014 — <1%
Publication

---

17 Shinohara, H.. "Partition of chlorine compounds between silicate melt and — <1%

hydrothermal solutions: I. Partition of NaCl-KCl", Geochimica et Cosmochimica Acta, 198910
Publication

18	www.researchgate.net Internet Source	<1 %

Exclude quotes	On	Exclude matches	Off
Exclude bibliography	On		